HELDA
HELSINGIN YLIOPISTO
HELSINGFORS UNIVERSITET
UNIVERSITY OF HELSINKI

UNIVERSITY OF HELSINKI

https://helda.helsinki.fi

Sub-100 mu m Spatial Resolution Ambient Mass Spectrometry Imaging of Rodent Brain with Laser Ablation Atmospheric Pressure Photoionization (LAAPPI) and Laser Ablation Electrospray Ionization (LAESI)

Hieta, Juha-Pekka

2020-10-20

Hieta , J-P , Kopra , J , Räikkönen , H , Kauppila , T & Kostiainen , R 2020 , ' Sub-100 mu m Spatial Resolution Ambient Mass Spectrometry Imaging of Rodent Brain with Laser Ablation Atmospheric Pressure Photoionization (LAAPPI) and Laser Ablation Electrospray Ionization (LAESI) ' , Analytical Chemistry , vol. 92 , no. 20 , pp. 13734-13741 . https://doi.org/10.1021/acs.analchem.0c01597

http://hdl.handle.net/10138/334367
https://doi.org/10.1021/acs.analchem.0c01597

acceptedVersion

Downloaded from Helda, University of Helsinki institutional repository.

This is an electronic reprint of the original article.

This reprint may differ from the original in pagination and typographic detail.

Please cite the original version.

Sub-100 µm spatial resolution ambient mass spectrometry imaging of rodent brain with laser ablation atmospheric pressure photoionization (LAAPPI) and laser ablation electrospray ionization (LAESI)

Juha-Pekka Hieta[†], Jaakko Kopra[‡], Heikki Räikkönen[†], Tiina J. Kauppila[§]*, Risto Kostiainen[†]*

[†] Drug Research Program and Division of Pharmaceutical Chemistry and Technology, Faculty of Pharmacy, P.O. Box 56, FI-00014 University of Helsinki, Finland

[‡] Division of Pharmacology and Pharmacotherapy, Faculty of Pharmacy, P.O. Box 56, FI-00014 University of Helsinki, Finland

[§] Finnish Institute for the Verification of the Chemical Weapons Convention (VERIFIN), Department of Chemistry, P.O. Box 55, FI-00014 University of Helsinki, Finland

risto.kostiainen@helsinki.fi, tiina.kauppila@helsinki.fi

ABSTRACT: In this study, we applied a new IR laser-beam-focusing technique to enable sub-100 µm spatial resolution in laser ablation atmospheric pressure photoionization (LAAPPI) and laser ablation electrospray ionization (LAESI) mass spectrometry imaging (MSI). After optimization of operational parameters, both LAAPPI- and LAESI-MSI with a spatial resolution of 70 µm produced high quality MS images, which allowed accurate localization of metabolites and lipids in the mouse and rat brain. Negative and positive ion LAAPPI- and LAESI-MS detected many of the same metabolites and lipids in the brain. Many compounds were also detected either by LAAPPI- or LAESI-MS, indicating that LAAPPI and LAESI are more complementary than alternative methods.

Mass spectrometry imaging (MSI)[1–3] is a molecular imaging technology that can be used to study and visualize the spatial distributions of compounds in solid samples. MSI is widely used for imaging of complex biological samples such as tissue sections of different organs[4,5] and whole-body animals[6,7] or now even single cells.[8] Modern high-resolution mass spectrometry (MS) allows simultaneous imaging of thousands of compounds, varying from small molecules such as drugs and metabolites to large biomolecules such as peptides and intact proteins.

The current commercial state-of-the-art MSI instruments typically incorporate matrix-assisted laser desorption/ionization (MALDI)[9] and vacuum sampling by ultraviolet (UV) laser, which enable imaging of the aforementioned compound classes.[10,11] However, vacuum sampling requires the samples to be dehydrated, UV photons can desorb material only from a sample surface,[12] and regular MALDI can produce relatively low ion yields for many compound classes.[13] Such limitations can be partly overcome with different MALDI variants, such as atmospheric pressure infrared (IR)-MALDI,[14] which provides efficient sampling without sample dehydration. The ion yields of the desorbed compounds can also be improved by using laser-induced post-ionization (MALDI-2).[15] However, all MALDI variants require samples to be coated with a chemical matrix and many additional sample treatment steps or protocols are typically recommended depending on the aim of analysis.[12,16,17]

In contrast, MSI-feasible, ambient, and matrix-free MS techniques,[18] such as desorption electrospray ionization (DESI),[19] can be applied for imaging of tissue sections without any further sample preparation. This reduces the chemical background in mass spectra and minimizes the degradation and migration of analytes in samples, which make ambient MSI a simple and straightforward method for tissue imaging. DESI-MS has become the most popular ambient MSI technique due to its simplicity, affordability, and capability for high throughput analysis. However, low repeatability and undesired adduct formation make DESI a challenging technique in measurements that require long-time stability, such as MSI.[20]

Laser ablation atmospheric pressure photoionization (LAAPPI)[21] and electrospray ionization (LAESI)[22] couple the benefits of IR laser-ablation sampling and ambient MS. LAAPPI- and LAESI-MS allow matrix-free MSI measurements[23,24] as the IR laser energy is absorbed by the sample water. The emitted IR photons can penetrate deeper into the tissue than UV photons,[25,26] resulting in improved sensitivity as a larger amount of material is sampled for post-ionization with APPI[27] or ESI.[28] Furthermore, IR laser enables sampling of compounds that reside at deeper parts of the sample. This is a major advantage, for example, in the MSI analysis of samples such as plant leaves, which cannot be sectioned or otherwise prepared. Moreover, APPI provides good ionization efficiency for nonpolar neutral compounds that may be poorly ionized by electrospray ionization. However, LAESI is suitable for the analysis of small and large biomolecules, whereas LAAPPI is suitable only for smaller molecules such as metabolites and lipids. Utilization of both techniques could therefore provide complementary biological information.

IR laser-ablation MSI, which includes LAAPPI, LAESI, and infrared matrix-assisted laser desorption electrospray ionization (IR-MALDESI)[29] techniques, has mainly been limited to a spatial resolution of 150–400 µm.[22,23,30–33] Commercial UV-MALDI can typically perform measurements in the range of 5–100 µm.[34,35] Recently, two different OPO IR laser-beam-focus-

ing techniques[36,37] have been reported that allow IR laser-ablation MSI with even 50-µm spatial resolution. Thus far, LAAPPI has been demonstrated in MSI of mouse brain,[36] whole sage leaves,[23] and birch bark[38] with 60-µm, 400-µm, and 400-µm spatial resolutions, respectively. On the other hand, LAESI has been widely used in MSI, such as in the analysis of whole rat brain,[30] bacterial colonies,[31] and *A. squarrosa* leaves.[26] However, these studies have used spatial resolutions significantly higher than 100 µm. Although LAAPPI has been demonstrated once with a spatial resolution of 60 µm,[36] the robustness of the method in long-term sub 100-µm spatial resolution MSI measurements of whole organ sections has not been shown. Furthermore, LAAPPI- and LAESI-MSI brain studies have only reported distributions of positive ions, and images in the negative ion mode have not been published.

Here, we present a comparison of 70-µm spatial resolution LAAPPI- and LAESI-MSI for mouse brain tissue analysis in positive and negative ion modes. The effects of the main operation parameters of both methods are described and the overall feasibilities of the techniques are compared in MSI of mouse brain tissue sections. Furthermore, the stability of the optimized LAAPPI-MS for imaging of larger sample areas is tested with a measurement of a whole rat brain section.

MATERIALS AND METHODS

Solvents. The following three spray solvents were tested in LAAPPI: acetone (CHROMASOLV, Honeywell Riedel-de Haën, Seelze, Germany), toluene (CHROMASOLV Plus, Sigma-Aldrich, Steinheim, Germany), and chlorobenzene (HPLC 99.9%, Sigma-Aldrich). The spray solution in LAESI was an 8:1 mixture of methanol (CHROMASOLV, Honeywell Riedel-de Haën, Seelze, Germany) and Milli-Q water (Merck Millipore, Molsheim, France) with 0.1% formic acid (EMSURE 98–100%, Merck, Darmstadt, Germany). The spray solvents were pumped using an Agilent 1100 capillary LC pump (Waldbronn, Germany).

Animals and Tissue Samples. All experiments were conducted following the 3R principles of the EU directive 2010/63/EU governing the care and use of experimental animals and were approved by the County Administrative Board of Southern Finland (license number ESAVI/12046/04.10.07/2017). The protocols were authorized by the national Animal Experiment Board of Finland. Two-month-old mice from a mixed genetic background (129Ola/ICR/C57bl6) were killed by decapitation. Their brains were removed and flash frozen by submersion into iso-pentane in a beaker cooled with dry ice. Afterwards, 20-, 40- and 60-µm thick coronal striatal sections were cut with a cryomicrotome (Leica CM 3050; Leica Microsystems Nussloch GmbH, Nussloch, Germany) operating at -10 °C. Several brain sections with different thicknesses were cut to investigate the effect of tissue thickness on acquired signal levels. All sections were collected and thaw-mounted onto normal microscope glass slides and stored at -80 °C before analysis.

Imaging Setup and Ion Sources. The full descriptions of the developed imaging setup and in-house built LAAPPI and LAESI sources are presented in the Supporting Information. Briefly, the imaging setup was built within a removable module to have a semi-closed space to control the relative humidity of the sample region with dry nitrogen flow. The temperature of the sample holder surface was kept below -20 °C to decrease the rate of dehydration and enzymatic and chemical reactions, such as oxidation in tissue. OPOTEK IR Opolette HE 2940 (Carlsbad, CA, USA) laser was used with a simple mirror setup described previously.[36] The mirror setup permitted setting of a specific sampling spot diameter (20–200 µm) solely by changing the beam travel distance before the focusing lens. Here, spot diameter of approximately 65 µm was selected due to its suitable accuracy for showing the structural details of rodent brain in a reasonable measurement timeframe.

The LAAPPI source (Figure 1) consisted of a heated stainless-steel (SS) pneumatic sprayer to produce a hot vapor jet and a krypton discharge vacuum ultraviolet (VUV) lamp (PKR 100; Heraeus Noblelight, Cambridge, UK) to emit 10.0 and 10.6eV photons for photoionization, whereas the LAESI source was based on a 100 µm I.D. SS electrospray needle (MT320-100-5-5; New Objective, MA, US) and an in-house built high voltage power supply to apply a voltage of (+/–) 2.1–2.3 kV for producing a steady cone-jet mode of electrospray. The mass spectrometer inlet glass capillary was equipped with a heated 24 mm long SS extension capillary. Capillary temperatures of 370 °C and 200 °C were used for LAAPPI and LAESI-MS, respectively.

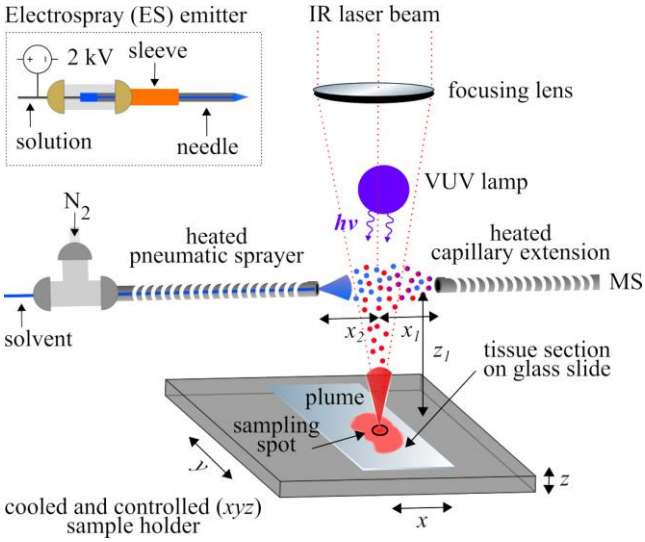

Figure 1. LAAPPI- and LAESI-MS setups. In LAESI-MS, the heated pneumatic sprayer is replaced with an ES emitter (top-left inset) and the VUV lamp is turned off.

Data Acquisition and Processing. The mass spectra were acquired using a Bruker micrOTOF focus mass spectrometer (Bremen, Germany) with a mass range of *m/z* 50–1200 and data acquisition frequency of 5 Hz. The instrument achieved a mass resolution of 9000–10000 at *m/z* 200–300. The drying gas flow around the MS inlet was turned off and the capillary exit and skimmers 1 and 2 voltages were set to (+/-) 116.7 V, 38.9 V, and 28.9 V, respectively. Hexapole RF of 60 Vpp was used for screening the entire *m/z* range and 300–600 Vpp for more focused analysis in the mass range *m/z* 500–1200. The IR laser output energy, repetition rate, and number of pulses for each sample spot were 6 mJ, 20 Hz, and 20, respectively.

All imaging measurements were automatically run by an in-house developed MATLAB-based program (2018a; The MathWorks Inc., Natick, Massachusetts, US) that controlled e.g., the raster scanning of the selected sample area(s), the triggering of the IR laser, and the temperature of the sample holder relative to the relative humidity around the analysis region. The spot-to-spot analysis dwell times varied between 2.5–3 s and 4–6 s in LAAPPI- and LAESI-MSI measurements, respectively. However, the typical signal durations in LAAPPI-MSI varied between 0.6–1.2 s and the set dwell time is the shortest feasible with the current software. On the other hand, the variations in the LAESI-MSI dwell times were caused by minor changes in

the setup, typically in the emitter position, or by the used spray solvent flow rate, which directly affected the signal durations. The parameters affecting the signal durations are discussed in more detail in the optimization section and in the Supporting Information. The current setup allows imaging with a rate of ~1200 pixels/h by LAAPPI-MS (or ~3000 pixels/h after software optimization, see the Supporting Information), whereas the rate of LAESI-MSI was typically only half of the rate of LAAPPI-MSI.

After analysis, the acquired data was automatically processed to pixel files that contained sum spectra generated from each measurement spot. The pixel files and ion images were created with a Python-based command-line tool. A free open-source MATLAB-based MSiReader[39] program was used for studying the MSI datasets. Level 5 identification[40] of detected compounds was performed by searching accurate masses against public online HMDB[41] and LIPID MAPS[42] databases as unambiguous structural characterization was not possible with TOF-MS. Only the major mass peaks detected by each technique are compared and matched with the major brain species reported in the literature.

RESULTS AND DISCUSSION

Optimization of LAAPPI- and LAESI-MS for Brain Tissue Analysis. The effects of ablation and ionization parameters were investigated to achieve maximum sensitivity and stability in MSI of the mouse brain using LAAPPI- and LAESI-MS. These parameters were: 1) positioning of the sprayer tip, the sampling spot, and the extension capillary in relation to each other; 2) the spray solvent, its flow rate, and the pressure and temperature of the nebulizer gas (nitrogen); and 3) the thickness and temperature of the sample and its state prior to analysis. All optimized ion source settings are summarized in Table 1 and the optimization results are presented in detail in the Supporting Information.

Briefly, the position of the sprayer tip in relation to the ablation plume, and the temperature of the sample were the parameters that most affected the stability in MSI. At close proximity to the ablation plume, the used ES emitter was prone to carry-over due to the adsorption of tissue residues on the emitter surface, whereas the heated nebulizer used in LAAPPI-MS did not suffer from memory effects regardless of its position. The carry-over with the ES emitter can be avoided by using longer emitter-plume distances, although this will reduce the sensitivity. Spot-to-spot sampling repeatability of frozen tissue was observed to be better than that of tissue at room temperature. This may be because the IR laser ablated frozen tissue produced (visually observed) finer plume than the non-frozen tissue. Sampling of frozen tissue required the relative humidity within the imaging module to be set to a specific value (Table 1) to avoid either condensation of water on tissue or dehydration of tissue during MSI measurements.

Positive and Negative Ion LAAPPI and LAESI Mass Spectra of Mouse Brain. Typical positive and negative ion LAAPPI- and LAESI-MS mass spectra acquired from the white matter region of mouse brain are presented in Figure 2, whereas their respective background spectra are presented in the Supporting Information (Figure S6). All proposed metabolites and lipids, mass errors, and abundances of the main ions are presented in Table S1. Many of the metabolites detected by positive ion LAESI-MS were also detected by LAAPPI-MS. However, positive ion LAAPPI mass spectra showed significantly more ions than LAESI, which is partly due to the stronger fragmentation of metabolites and lipids by APPI. Many of the fragments in the positive ion LAAPPI spectra, especially in the mass range of *m/z* 500–700, are suggested to result from fragmentation of phospholipids and sphingolipids. Below *m/z* 500, the majority of mass peaks detected by LAAPPI-MS are unlikely to be fragments, as peaks with similar accurate masses are also observed in LAESI-MS spectra. Both techniques also detected many lipids in the mass range of *m/z* 700–1000, but with different peak patterns. In contrast to positive ion mode, negative ion spectra of LAESI and LAAPPI at the mass range below *m/z* 500 show many different ions.

Table 1. Optimal LAAPPI and LAESI Ion Source Parameters for MSI of Mouse Brain Tissue Sections.

Parameter	LAAPPI	LAESI
Spot-inlet distance (x_1)	4–6 mm	4–6 mm
Spot-sprayer distance (x_2)	~1 mm	~1 mm
Sample-inlet axis distance (z_1)	6–8 mm	6–8 mm
Spray temperature	350–450 °C	Ambient
Nebulizer gas pressure	0.4–0.8 MPa	-
Solvent flow rate	1–5 µL min^{-1}	3 µL min^{-1}
Sample thickness	40 µm	20 µm
Relative humidity in module / sample holder temperature	6–7 % / -22 °C	3–4 % / -22 °C

Both positive ion LAAPPI- and LAESI-MS below *m/z* 500 can detect abundant metabolites of mouse brain, including γ-aminobutyric acid (GABA, m/z 104.07), creatine (*m/z* 132.07), aspartic acid (*m/z* 134.04), spermidine (*m/z* 146.17), glutamine (*m/z* 147.08), glutamic acid (*m/z* 148.06), N-acetylaspartic acid (*m/z* 176.06), and cholesterol (*m/z* 369.35), with significantly different sensitivities between methods (Table S1). LAESI-MS is also suggested to detect GABA (*m/z* 104.07) and choline (*m/z* 104.11) as separated mass peaks (Figure S7) and taurine and glutathione at *m/z* 126.02 and 308.09, respectively. In addition, phosphate-containing compounds such as adenosine monophosphate (*m/z* 348.07) and several phospholipid fragment ions, including phosphoethanolamine (*m/z* 142.03), were only detected with LAESI-MS. Several fragment ions in the mass ranges of *m/z* 100–350 and *m/z* 500–700 were detected by LAAPPI-MS due to its more energetic ionization process compared to LAESI. Many of the metabolites and lipids were also detected as their $[M+H-H_2O]^+$ fragments in LAAPPI-MS, such as: N-acetylaspartic acid (*m/z* 176.06); glutamic acid (*m/z* 148.06); threonine (*m/z* 120.07); creatine (*m/z* 132.08); and monoacylglycerides (MG), including MG(16:0) (*m/z* 313.27), MG(18:1) (*m/z* 339.29), and MG(18:0) (*m/z* 341.30). LAAPPI produced several intense fragments in the mass range of *m/z* 500–700, such as ceramide Cer(d36:1) at *m/z* 548.54 and diglyceride DG(36:1) at *m/z* 605.55, which are most likely formed by fragmentation of sphingolipid and phospholipid head groups together with one water molecule.

LAESI and LAAPPI mass spectra in the mass range of *m/z* 700–1000 showed several significantly different lipid patterns between methods. The lipid classes detected by either or both methods in positive or negative ion mode are summarized below (Figure 3). In positive ion mode, phosphatidylcholines (PC) and sphingomyelins (SM) were detected only by LAESI-MS, phosphatidylethanolamines (PE) by both techniques, and galactosylceramides (GalCer) were detected only with LAAPPI-MS (Table S1). PCs are efficiently ionized by ESI and their protonated molecules, such as PC(32:0) (*m/z* 734.57) and PC(34:1) (*m/z* 760.59), were detected with high abundance. LAESI

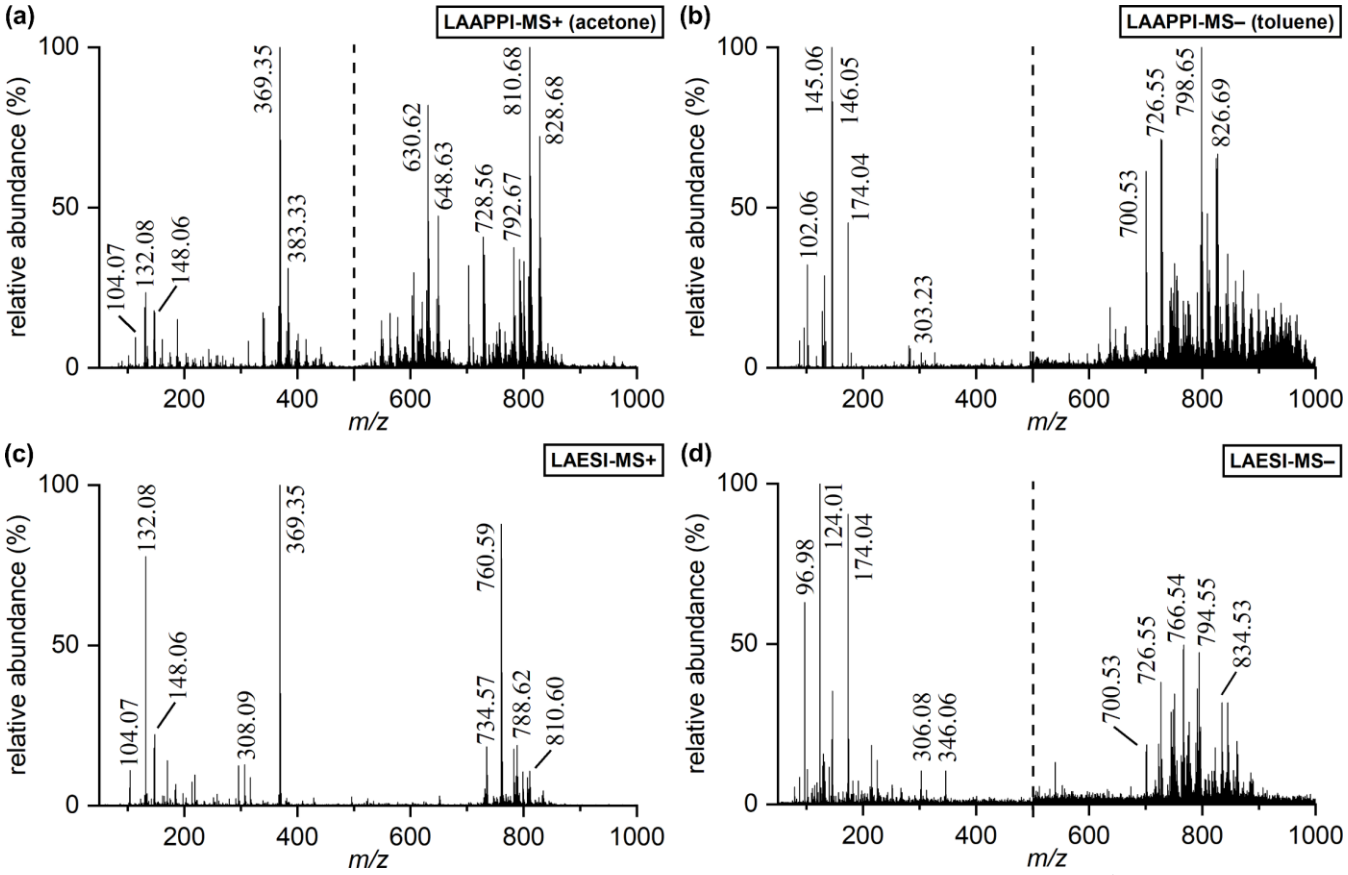

Figure 2. Background subtracted positive and negative ion LAAPPI- and LAESI-MS mass spectra (a–d) acquired from white matter region of mouse brain. Figures (a), (b), and (d) consist of two measurements that are separated with a dashed line.

spectra showed some relatively weak ions at odd-numbered *m/z* values that match with protonated sphingomyelin (SM) species, such as SM(d36:2) at *m/z* 729.59 and SM(d36:1) at *m/z* 731.61. Several PEs were detected with both techniques, but the relative abundances with LAAPPI-MS are typically higher than with LAESI-MS. For example, PE(34:0), PE(38:6), and PE(40:7) were detected with both techniques as protonated molecules at *m/z* 720.55, 764.52, and 790.54, respectively. Many of the PE lipids have the closest accurate mass database matches with ethanolamine plasmalogens (PEP), a subclass of PE that accounts for at least one half of all PE lipids in whole brain[43] and about 85% in myelin.[44] For example, the intense ions in LAAPPI mass spectra at *m/z* 702.54, 728.56, and 730.58 match with PE(P-34:1), PE(P-36:2), and PE(P-36:1), respectively, which are also among the major PEP species of the brain.[45] GalCer were detected with high relative abundance with LAAPPI-MS but not with LAESI-MS. The white matter regions of the brain contain a large number of glycolipids in its myelin sheet, which comprise about 30% of its lipid mass.[46] Glycolipids of the brain also contain either a non-hydroxy or 2-hydroxy fatty acid of which the α-hydroxylated species constitute approximately 60% of all GalCer in the mature rat brain.[47,48] Mass peaks matching with GalCer with both fatty acid species were detected by positive ion LAAPPI-MS as either protonated molecules or $[M+H–H_2O]^+$ fragment ions based on the accurate masses. The detection of GalCer species is supported by the large number of simultaneously observed ceramide fragments, such as Cer(d42:2), detected as $[Cer(d42:2)+H–H_2O]^+$ at *m/z* 630.62, and Cer(d42:1(OH)), detected as $[Cer(d42:1(OH))+H]^+$ at *m/z* 666.64.

At the mass range below *m/z* 500, both negative ion LAESI and LAAPPI mass spectra (Table S1) showed alanine (*m/z* 88.04), lactic acid (*m/z* 89.02), GABA (*m/z* 102.06), serine (*m/z* 104.04), threonine (*m/z* 118.05), creatine (*m/z* 130.06), aspartic acid (*m/z* 132.03), glutamine (*m/z* 145.06), glutamic acid (*m/z* 146.04), N-acetyl-L-aspartic acid (*m/z* 174.04), and hexose (*m/z* 179.06) as deprotonated molecules. In addition, LAESI-MS detected phosphate (*m/z* 96.97), taurine (*m/z* 124.01), malic acid (*m/z* 133.01), histidine (*m/z* 154.06), ascorbic acid (*m/z* 175.03), glutathione (*m/z* 306.08), and adenosine monophosphate (*m/z* 346.06) as deprotonated molecules. Both techniques also detected several lipid fragments at low mass range. While LAESI spectra contained mass peaks that match with deprotonated phospholipid head groups, such as phosphorylethanolamine at *m/z* 140.02, LAAPPI spectra showed deprotonated fatty acids such as stearic (18:0) (*m/z* 283.26) and arachidonic (24:4) (*m/z* 303.23) acid. LAAPPI spectra at the mass range *m/z* 500–700 also showed that glycolipid fragments formed from α-hydroxylated or non-hydroxylated GalCer species, such as Cer(d40:1(OH)) at *m/z* 636.59 and Cer(d42:2) at *m/z* 646.61.

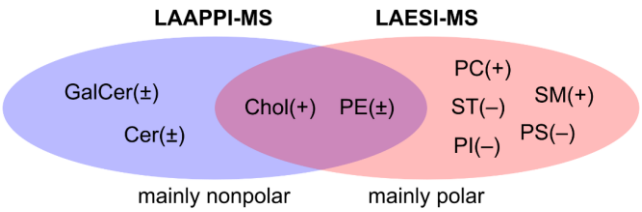

Figure 3. Lipid classes detected by positive (+) and negative (–) ion LAAPPI- and LAESI-MS. (GalCer = galactosylceramide, Cer = ceramide, Chol = cholesterol, PE = phosphatidylethanolamine, PC = phosphatidylcholine, SM = sphingomyelin, ST = sulfatide, PS = phosphatidylserine, PI = phosphatidylinositol).

At the mass range of *m/z* 700–1000, negative ion LAAPPI and LAESI spectra (Table S1) included many of the same mass

peaks of PE plasmalogen and diacyl species, such as deprotonated PE(P-36:2) at *m/z* 726.55 and PE(40:6) at *m/z* 790.55. Both techniques also detected many GalCer species from white matter as chlorinated adducts, but only LAAPPI-MS detected GalCer species as deprotonated molecules. Deprotonated GalCer peaks in LAAPPI-MS spectra were, however, one or two orders of magnitude higher than the adduct signals observed with LAESI-MS. Phosphatidylserine (PS) and phosphatidylinositol (PI) species including deprotonated PS(40:6) at *m/z* 834.53 and deprotonated PI(38:4) at *m/z* 885.55 were detected only with LAESI-MS. The detection of these species were expected as in the brain about 51% of the total PS content consists of PS(40:6) and about 60% of the total PI content consists of PI(38:4) species.[45] LAESI-MS also showed few abundant sulfated GalCer species (i.e. sulfatides, ST) such as deprotonated ST(24:1) at *m/z* 888.62.

When comparing our experiments in both ion modes, we conclude that PE and GalCer species can be detected with positive and negative ion modes; PS, PI, and ST species only in negative ion mode; and PC and SM species only in positive ion mode. In principle, all zwitterionic (such as PC, PE, and SM) or neutral phospholipids (such as GalCer) can be ionized in both positive and negative ion modes, but those including a quaternary ammonium group are ionized significantly more efficiently in positive ion mode than in negative ion mode. Anionic phospholipids, such as PI and ST, are ionized more efficiently in negative ion mode.[49] These results are consistent with the findings of earlier lipidomics studies with ESI-[45,50,51] and APPI-MS.[52]

Mass Spectrometry Imaging of Rodent Brain. LAAPPI and LAESI MS imaging (MSI) utilized a recently introduced OPO IR laser beam focusing method that allows an approximate 10-fold decrease to the typical 200–400 µm resolution achieved thus far in IR laser-ablation-based MSI.[36] Here, spatial resolution below 100 µm (70 µm) was applied for the first time in negative ion LAAPPI- and LAESI-MS imaging and in LAAPPI-MS imaging of a whole rat brain tissue section. Although better spatial resolution could be achieved, the selected 70 µm resolution allows a compromise between the speed of analysis and the quality of ion images. For example, significantly more accurate distributions of adenosine (*m/z* 268.10) and PC(37:6) (*m/z* 792.55) in Figures 4c and 4g were acquired by positive ion LAESI-MS with 70-µm spatial resolution than achieved earlier for the same ions using LAESI with 200-µm spatial resolution.[30]

In addition to spatial resolution, spot-to-spot repeatability affects the quality of ion images. Good spot-to-spot repeatability is indicated by the total ion current (TIC) traces and by the selected ion traces of *m/z* 148.06 (glutamic acid, GA) acquired from mouse brain tissue sections by positive ion LAAPPI- and LAESI-MS (Figure S8). However, LAESI is more prone to cause carry-over than LAAPPI, especially with short emitter-to-plume distances as discussed in detail in the Supporting Information. The effect of carry-over is demonstrated in positive and negative ion LAESI images of PE(P-36:2) (Figures 4d and 4e), especially around the corpus callosum. This problem can be minimized either by moving the tip of the ES emitter to a longer distance from the ablated plume at the cost of sensitivity (Figure 4a, c, e, f, and g) or by increasing the dwell time between the analyses of spots at the cost of total analysis times. As LAAPPI uses a heated nebulizer, no carry-over effect caused by contamination of the sprayer is observed, and LAAPPI-MS can be used without compromising sensitivity or analysis times.

The distributions of small metabolites and lipids that show a specific localization pattern in the measured tissue sections also match well with different regions or structures of mouse and rat brain (Figures 4 and 5). For example, the LAAPPI-MS image of *m/z* 810.68 in mouse brain (Figure 4h), and *m/z* 826.68 and *m/z* 754.62 in rat brain (Figure 5) show patterns that match with the myelinated parts of the brain (Figure 4i).[53] This indicates that GalCer(d42:1), GalCer(d42:1(OH)), and GalCer(d38:1), respectively, have the highest concentration in the corpus callosum (CC), which is the largest white matter structure in the brain. On the other hand, the concentration of PC(37:6) in mouse brain (Figure 4g) or PE (34:0) in rat brain (Figure 5) is clearly lower in the CC than in the cerebral cortex (CTX) or thalamus (TH). Conversely, the concentration of adenosine and PE(P-36:4) are higher in the thalamus than in other regions of the mouse brain (Figures 4c and 4f). Furthermore, the elevated concentration of GABA in the hypothalamus is clearly detected in the LAESI image of ion *m/z* 104.07 (Figure 4a), which is consistent with earlier works.[30,54,55] These results show that our new method[36] for improving the spatial resolution can be used to determine accurate distributions of metabolites and lipids in rodent brain tissue sections by LAAPPI- and LAESI-MS.

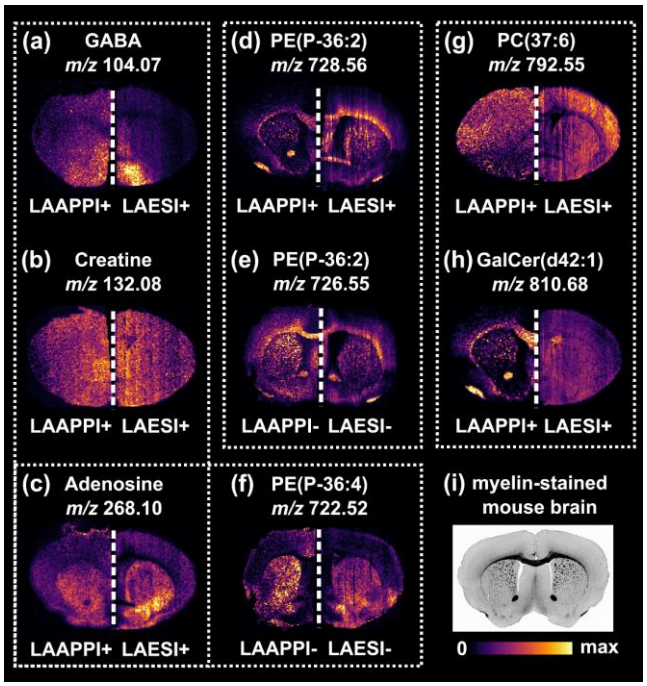

Figure 4. LAAPPI and LAESI MS images of mouse brain (a–h) acquired with 70-µm spatial resolution, and an image (i)[53] showing a myelin-stained mouse brain section.

In general, the metabolites and lipids, which can be detected with LAAPPI- and LAESI-MS, also show similar distributions in mouse brain tissue sections (Figures 4a–f). For example, the ion images of PE(P-36:2) detected at *m/z* 728.56 and 726.54 in positive and negative ion mode, respectively (Figures 4d and 4e), and the images of adenosine (*m/z* 286.10) and PE(P-36:4) (*m/z* 722.52) (Figures 4c and 4f) show similar distributions with both techniques. On the other hand, LAAPPI and LAESI provide complementary data, as some metabolites can be detected only with either LAAPPI- or LAESI-MS. For example, GABA (*m/z* 104.07) and PC(37:6) (*m/z* 792.55) show distinctive distributions only with LAESI-MS (Figures 4a and 4c), whereas GalCer(d42:1) (*m/z* 810.68) shows a clear distribution only with LAAPPI-MS (Figure 4h). Many small metabolites and lipids were also distributed similarly but without any specific pattern across the mouse brain sections. Such a distribution is presented

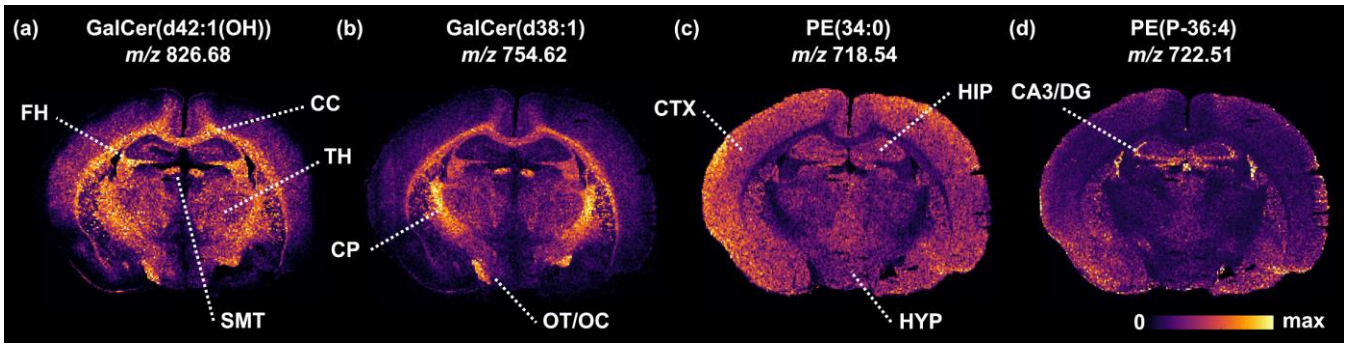

Figure 5. Negative ion LAAPPI images (a–d) of a 20-µm thick whole rat brain tissue section measured with 70-µm spatial resolution. (CC = corpus callosum, SMT = stria medullaris of the thalamus, FH = fimbria of the hippocampus, TH = thalamus, CP = corticofugal pathways, OT/OC = optical tract and chiasm, CTX = cerebral cortex, HYP = hypothalamic region, HIP = hippocampal region, CA3 = field of Ammon's horn, DG = dentate gyrus)

with an ion image of creatine (Figure 4b) but also e.g., a phospholipid PC(34:1) detected at *m/z* 760.59 (not shown) by positive ion LAESI-MS had a uniform distribution in the measured mouse brain sections as shown similarly by Nemes et al.[30]

The ability of the LAAPPI-MSI platform was further investigated for the imaging of a 20-µm thick whole rat brain tissue section in negative ion mode. As rat brains are larger than mouse brains, different parts of the brain can be more clearly visualized as a higher number of pixels can be measured from each part. On the other hand, the imaging of a larger area requires long-term stability of the measurement technique, for which LAAPPI-MS is well suited as it provides good robustness for the analysis without memory effects. The MS images of metabolites and lipids in rat brain that are measured with a spatial resolution of 70 µm now consisted of nearly 30000 pixels. For example, the distributions of four lipids each highlighting different regions of rat brain are presented in Figure 5. The ion image of a α-hydroxylated GalCer(42:1) species (Figure 5a) shows that this glycolipid is quite evenly distributed in all white matter regions of rat brain, including CC, stria medullaris of the thalamus (SMT), fimbria of the hippocampus (FH), and the myelinated parts of thalamus (TH). On the other hand, another white matter specific glycolipid, a non-hydroxylated GalCer(38:1) (Figure 5b), has the highest concentration especially in the regions of corticofugal pathways (CP) and optical tract and chiasm (OT/OC). In contrast to glycolipids, the distribution of a phospholipid PE(34:0) (Figure 5c) shows that this species exists more abundantly in gray matter regions of rat brain, such as cerebral cortex (CTX) and hippocampus (HIP). One of the most interesting discoveries, however, was that the spatial resolution of 70 µm was sufficient to distinguish even smaller regions of rat brain. For instance, the distribution of a PE plasmalogen species PE(P-36:4) (Figure 5d) clearly shows the highest concentration at the outer parts of the hippocampal region, such as CA3 of Ammon's horn and dentate gyrus (DG) and at the lower parts of the CTX.

CONCLUSIONS

The most important advantage of LAAPPI- and LAESI-MSI is their ability to image tissue sections with no need for further sample treatment steps, such as dehydration or addition of chemical matrix, which are required with commercial vacuum UV-MALDI-MSI instruments. Optimization of operational parameters in LAAPPI- and LAESI-MS experiments was shown to be necessary to obtain high sensitivity, good spot-to-spot repeatability, and robustness of analysis and thus high-quality MS images. Many of the same metabolites and lipids were detected from mouse brain tissue sections with LAAPPI- and LAESI-MS in both ion modes, but also a significant number of the compounds were detected by either LAAPPI- or LAESI-MS, in either positive or negative ion mode. Both techniques had clear advantages in the analysis of brain tissue samples and the technique and ion mode should be chosen on the basis of the research goal.

As commonly used OPO IR lasers can be now focused down to significantly smaller spots than was previously possible, LAAPPI- and LAESI-MS can produce MS images with quality that is closer to that of UV-MALDI-MSI. Both LAAPPI- and LAESI-MSI allowed accurate localization of metabolites and lipids in the mouse and rat brain tissue sections. In many cases, the distributions of compounds matched well with different regions of the brain. In addition to positive ion mode, we applied LAAPPI- and LAESI-MS for the first time in negative ion mode for mouse brain imaging. In addition, the feasibility of negative ion LAAPPI-MS was tested with a spatial resolution of 70 µm in imaging of a whole rat brain tissue section. LAAPPI-MS was shown to be robust during the entire measurement and collection of nearly 30 000 pixels and it produced high-quality MS images that enabled detailed localization of metabolites and lipids in rat brain.

ASSOCIATED CONTENT

Supporting Information

Full descriptions of imaging setup and ion sources, complete optimization results, and Figures S1–S8 and Table S1.

AUTHOR INFORMATION

Corresponding Author

*Email: risto.kostiainen@helsinki.fi. Tel. +358-294159134
*Email: tiina.kauppila@helsinki.fi. Tel. +358-294150418

Author Contributions

All authors contributed to the writing of the manuscript, and all authors gave their approval to the final version of the manuscript.

Notes

The authors declare no competing financial interest.

ACKNOWLEDGMENT

Academy of Finland (projects #275089, #2515752, #276627, and #1321472) is acknowledged for funding. The authors thank Kati Rautio and Suvi Pöyhönen for preparation of mouse and rat brain tissue sections, respectively.

REFERENCES

(1) Buchberger, A. R.; DeLaney, K.; Johnson, J.; Li, L. Mass Spectrometry Imaging: A Review of Emerging Advancements

and Future Insights. *Anal. Chem.* **2018**, *90* (1), 240–265. https://doi.org/10.1021/acs.analchem.7b04733.

(2) McDonnell, L. A.; Heeren, R. M. A. Imaging Mass Spectrometry. *Mass Spectrom. Rev.* **2007**, *26* (4), 606–643. https://doi.org/10.1002/mas.20124.

(3) Gilmore, I. S.; Heiles, S.; Pieterse, C. L. Metabolic Imaging at the Single-Cell Scale: Recent Advances in Mass Spectrometry Imaging. *Annu. Rev. Anal. Chem.* **2019**, *12* (1), 201–224. https://doi.org/10.1146/annurev-anchem-061318-115516.

(4) Stoeckli, M.; Staab, D.; Staufenbiel, M.; Wiederhold, K. H.; Signor, L. Molecular Imaging of Amyloid β Peptides in Mouse Brain Sections Using Mass Spectrometry. *Anal. Biochem.* **2002**, *311* (1), 33–39. https://doi.org/10.1016/S0003-2697(02)00386-X.

(5) Stoeckli, M.; Chaurand, P.; Hallahan, D. E.; Caprioli, R. M. Imaging Mass Spectrometry: A New Technology for the Analysis of Protein Expression in Mammalian Tissues. *Nat. Med.* **2001**, *7* (4), 493–496. https://doi.org/10.1038/86573.

(6) Khatib-Shahidi, S.; Andersson, M.; Herman, J. L.; Gillespie, T. A.; Caprioli, R. M. Direct Molecular Analysis of Whole-Body Animal Tissue Sections by Imaging MALDI Mass Spectrometry. *Anal. Chem.* **2006**, *78* (18), 6448–6456. https://doi.org/10.1021/ac060788p.

(7) Huber, K.; Khamehgir-Silz, P.; Schramm, T.; Gorshkov, V.; Spengler, B.; Römpp, A. Approaching Cellular Resolution and Reliable Identification in Mass Spectrometry Imaging of Tryptic Peptides. *Anal. Bioanal. Chem.* **2018**, *410* (23), 5825–5837. https://doi.org/10.1007/s00216-018-1199-z.

(8) Lanni, E. J.; Rubakhin, S. S.; Sweedler, J. V. Mass Spectrometry Imaging and Profiling of Single Cells. *J. Proteomics* **2012**, *75* (16), 5036–5051. https://doi.org/10.1016/j.jprot.2012.03.017.

(9) Karas, M.; Hillenkamp, F. Laser Desorption Ionization of Proteins with Molecular Masses Exceeding 10,000 Daltons. *Anal. Chem.* **1988**, *60* (20), 2299–2301. https://doi.org/10.1021/ac00171a028.

(10) Shanta, S. R.; Kim, T. Y.; Hong, J. H.; Lee, J. H.; Shin, C. Y.; Kim, K. H.; Kim, Y. H.; Kim, S. K.; Kim, K. P. A New Combination MALDI Matrix for Small Molecule Analysis: Application to Imaging Mass Spectrometry for Drugs and Metabolites. *Analyst* **2012**, *137* (24), 5757–5762. https://doi.org/10.1039/c2an35782h.

(11) Caprioli, R. M.; Farmer, T. B.; Gile, J. Molecular Imaging of Biological Samples: Localization of Peptides and Proteins Using MALDI-TOF MS. *Anal. Chem.* **1997**, *69* (23), 4751–4760. https://doi.org/10.1021/ac970888i.

(12) Dong, Y.; Li, B.; Malitsky, S.; Rogachev, I.; Aharoni, A.; Kaftan, F.; Svatoš, A.; Franceschi, P. Sample Preparation for Mass Spectrometry Imaging of Plant Tissues: A Review. *Front. Plant Sci.* **2016**, *7* (60). https://doi.org/10.3389/fpls.2016.00060.

(13) Dreisewerd, K. The Desorption Process in MALDI. *Chem. Rev.* **2003**, *103* (2), 395–426. https://doi.org/10.1021/cr010375i.

(14) Römpp, A.; Schäfer, K. C.; Guenther, S.; Wang, Z.; Köstler, M.; Leisner, A.; Paschke, C.; Schramm, T.; Spengler, B. High-Resolution Atmospheric Pressure Infrared Laser Desorption/Ionization Mass Spectrometry Imaging of Biological Tissue. *Anal. Bioanal. Chem.* **2013**, *405* (22), 6959–6968. https://doi.org/10.1007/s00216-013-7180-y.

(15) Niehaus, M.; Soltwisch, J.; Belov, M. E.; Dreisewerd, K. Transmission-Mode MALDI-2 Mass Spectrometry Imaging of Cells and Tissues at Subcellular Resolution. *Nat. Methods* **2019**, *16* (9), 925–931. https://doi.org/10.1038/s41592-019-0536-2.

(16) Cillero-Pastor, B.; Heeren, R. M. A. Matrix-Assisted Laser Desorption Ionization Mass Spectrometry Imaging for Peptide and Protein Analyses: A Critical Review of on-Tissue Digestion. *J. Proteome Res.* **2014**, *13* (2), 325–335. https://doi.org/10.1021/pr400743a.

(17) Zemski Berry, K. A.; Hankin, J. A.; Barkley, R. M.; Spraggins, J. M.; Caprioli, R. M.; Murphy, R. C. MALDI Imaging of Lipid Biochemistry in Tissues by Mass Spectrometry. *Chem. Rev.* **2011**, *111* (10), 6491–6512. https://doi.org/10.1021/cr200280p.

(18) Wu, C.; Dill, A. L.; Eberlin, L. S.; Cooks, R. G.; Ifa, D. R. Mass Spectrometry Imaging under Ambient Conditions. *Mass Spectrom. Rev.* **2013**, *32* (3), 218–243. https://doi.org/10.1002/mas.21360.

(19) Takats, Z.; Wiseman, J. M.; Gologan, B.; Cooks, R. G. Mass Spectrometry Sampling Under Ambient Conditions with Desorption Electrospray Ionization. *Science.* **2004**, *306* (5695), 471–473. https://doi.org/10.1126/science.1104404.

(20) Gurdak, E.; Green, F. M.; Rakowska, P. D.; Seah, M. P.; Salter, T. L.; Gilmore, I. S. VAMAS Interlaboratory Study for Desorption Electrospray Ionization Mass Spectrometry (DESI MS) Intensity Repeatability and Constancy. *Anal. Chem.* **2014**, *86* (19), 9603–9611. https://doi.org/10.1021/ac502075t.

(21) Vaikkinen, A.; Shrestha, B.; Kauppila, T. J.; Vertes, A.; Kostiainen, R. Infrared Laser Ablation Atmospheric Pressure Photoionization Mass Spectrometry. *Anal. Chem.* **2012**, *84* (3), 1630–1636. https://doi.org/10.1021/ac202905y.

(22) Nemes, P.; Vertes, A. Laser Ablation Electrospray Ionization for Atmospheric Pressure, in Vivo, and Imaging Mass Spectrometry. *Anal. Chem.* **2007**, *79* (21), 8098–8106. https://doi.org/10.1021/ac071181r.

(23) Vaikkinen, A.; Shrestha, B.; Koivisto, J.; Kostiainen, R.; Vertes, A.; Kauppila, T. J. Laser Ablation Atmospheric Pressure Photoionization Mass Spectrometry Imaging of Phytochemicals from Sage Leaves. *Rapid Commun. Mass Spectrom.* **2014**, *28* (23), 2490–2496. https://doi.org/10.1002/rcm.7043.

(24) Zou, J.; Talbot, F.; Tata, A.; Ermini, L.; Franjic, K.; Ventura, M.; Zheng, J.; Ginsberg, H.; Post, M.; Ifa, D. R.; et al. Ambient Mass Spectrometry Imaging with Picosecond Infrared Laser Ablation Electrospray Ionization (PIR-LAESI). *Anal. Chem.* **2015**, *87* (24), 12071–12079. https://doi.org/10.1021/acs.analchem.5b02756.

(25) Zhigilei, L. V.; Garrison, B. J. Molecular Dynamics Simulation Study of the Fluence Dependence of Particle Yield and Plume Composition in Laser Desorption and Ablation of Organic Solids. *Appl. Phys. Lett.* **1999**, *74* (9), 1341–1343. https://doi.org/10.1063/1.123544.

(26) Nemes, P.; Barton, A. A.; Li, Y.; Vertes, A. Ambient Molecular Imaging and Depth Profiling of Live Tissue by Infrared Laser Ablation Electrospray Ionization Mass Spectrometry. *Anal. Chem.* **2008**, *80* (12), 4575–4582. https://doi.org/10.1021/ac8004082.

(27) Robb, D. B.; Covey, T. R.; Bruins, A. P. Atmospheric Pressure Photoionization: An Ionization Method for Liquid Chromatography-Mass Spectrometry. *Anal. Chem.* **2000**, *72* (15), 3653–3659. https://doi.org/10.1021/ac0001636.

(28) Fenn, J. B.; Mann, M.; Meng, C. K.; Wong, S. F.; Whitehouse, C. M. Electrospray Ionization for Mass Spectrometry of Large Biomolecules. *Science.* **1989**, *246* (4926), 64–71. https://doi.org/10.1126/science.2675315.

(29) Robichaud, G.; Barry, J. A.; Muddiman, D. C. IR-MALDESI Mass Spectrometry Imaging of Biological Tissue Sections Using Ice as a Matrix. *J. Am. Soc. Mass Spectrom.* **2014**, *25* (3), 319–328. https://doi.org/10.1007/s13361-013-0787-6.

(30) Nemes, P.; Woods, A. S.; Vertes, A. Simultaneous Imaging of Small Metabolites and Lipids in Rat Brain Tissues at Atmospheric Pressure by Laser Ablation Electrospray Ionization Mass Spectrometry. *Anal. Chem.* **2010**, *82* (3), 982–988. https://doi.org/10.1021/ac902245p.

(31) Li, H.; Balan, P.; Vertes, A. Molecular Imaging of Growth, Metabolism, and Antibiotic Inhibition in Bacterial Colonies by Laser Ablation Electrospray Ionization Mass Spectrometry. *Angew. Chemie Int. Ed.* **2016**, *55* (48), 15035–15039. https://doi.org/10.1002/anie.201607751.

(32) Etalo, D. W.; de Vos, R. C. H.; Joosten, M. H. A. J.; Hall, R. D. Spatially-Resolved Plant Metabolomics: Some Potentials and Limitations of Laser-Ablation Electrospray Ionization (LAESI) Mass Spectrometry Metabolite Imaging. *Plant Physiol.* **2015**, *169* (3), 1424–1435. https://doi.org/10.1104/pp.15.01176.

(33) Bagley, M. C.; Ekelöf, M.; Rock, K.; Patisaul, H.; Muddiman, D. C. IR-MALDESI Mass Spectrometry Imaging of Underivatized Neurotransmitters in Brain Tissue of Rats Exposed to Tetrabromobisphenol A. *Anal. Bioanal. Chem.* **2018**, *410* (30), 7979–7986. https://doi.org/10.1007/s00216-018-1420-0.

(34) Bodzon-Kulakowska, A.; Suder, P. Imaging Mass Spectrometry: Instrumentation, Applications, and Combination with Other Visualization Techniques. *Mass Spectrom. Rev.* **2016**, *35* (1), 147–169. https://doi.org/10.1002/mas.21468.

(35) Angel, P. M.; Caprioli, R. M. Matrix-Assisted Laser Desorption Ionization Imaging Mass Spectrometry: In Situ Molecular Mapping. *Biochemistry* **2013**, *52* (22), 3818–3828. https://doi.org/10.1021/bi301519p.

(36) Hieta, J.-P.; Vaikkinen, A.; Auno, S.; Räikkönen, H.; Haapala, M.; Scotti, G.; Kopra, J.; Piepponen, P.; Kauppila, T. J. A Simple Method for Improving the Spatial Resolution in Infrared Laser Ablation Mass Spectrometry Imaging. *J. Am. Soc. Mass*

Spectrom. **2017**, *28* (6), 1060–1065. https://doi.org/10.1007/s13361-016-1578-7.

(37) Bokhart, M. T.; Manni, J.; Garrard, K. P.; Ekelöf, M.; Nazari, M.; Muddiman, D. C. IR-MALDESI Mass Spectrometry Imaging at 50 Micron Spatial Resolution. *J. Am. Soc. Mass Spectrom.* **2017**, *28* (10), 2099–2107. https://doi.org/10.1007/s13361-017-1740-x.

(38) Räsänen, R. M.; Hieta, J. P.; Immanen, J.; Nieminen, K.; Haavikko, R.; Yli-Kauhaluoma, J.; Kauppila, T. J. Chemical Profiles of Birch and Alder Bark by Ambient Mass Spectrometry. *Anal. Bioanal. Chem.* **2019**, *411* (28), 7573–7583. https://doi.org/10.1007/s00216-019-02171-9.

(39) Robichaud, G.; Garrard, K. P.; Barry, J. A.; Muddiman, D. C. MSiReader: An Open-Source Interface to View and Analyze High Resolving Power MS Imaging Files on Matlab Platform. *J. Am. Soc. Mass Spectrom.* **2013**, *24* (5), 718–721. https://doi.org/10.1007/s13361-013-0607-z.

(40) Schymanski, E. L.; Jeon, J.; Gulde, R.; Fenner, K.; Ruff, M.; Singer, H. P.; Hollender, J. Identifying Small Molecules via High Resolution Mass Spectrometry: Communicating Confidence. *Environ. Sci. Technol.* **2014**, *48* (4), 2097–2098. https://doi.org/10.1021/es5002105.

(41) Wishart, D. S.; Feunang, Y. D.; Marcu, A.; Guo, A. C.; Liang, K.; Vázquez-Fresno, R.; Sajed, T.; Johnson, D.; Li, C.; Karu, N.; et al. HMDB 4.0: The Human Metabolome Database for 2018. *Nucleic Acids Res.* **2018**, *46* (D1), D608–D617. https://doi.org/10.1093/nar/gkx1089.

(42) Sud, M.; Fahy, E.; Cotter, D.; Brown, A.; Dennis, E. A.; Glass, C. K.; Merrill, A. H.; Murphy, R. C.; Raetz, C. R. H.; Russell, D. W.; et al. LMSD: LIPID MAPS Structure Database. *Nucleic Acids Res.* **2007**, *35* (Database), D527–D532. https://doi.org/10.1093/nar/gkl838.

(43) Nagan, N.; Zoeller, R. A. Plasmalogens: Biosynthesis and Functions. *Prog. Lipid Res.* **2001**, *40* (3), 199–229. https://doi.org/10.1016/S0163-7827(01)00003-0.

(44) Han, X.; Holtzman, D. M.; McKeel, D. W. Plasmalogen Deficiency in Early Alzheimer's Disease Subjects and in Animal Models: Molecular Characterization Using Electrospray Ionization Mass Spectrometry. *J. Neurochem.* **2001**, *77* (4), 1168–1180. https://doi.org/10.1046/j.1471-4159.2001.00332.x.

(45) Choi, J.; Yin, T.; Shinozaki, K.; Lampe, J. W.; Stevens, J. F.; Becker, L. B.; Kim, J. Comprehensive Analysis of Phospholipids in the Brain, Heart, Kidney, and Liver: Brain Phospholipids Are Least Enriched with Polyunsaturated Fatty Acids. *Mol. Cell. Biochem.* **2018**, *442* (1–2), 187–201. https://doi.org/10.1007/s11010-017-3203-x.

(46) Norton, W. T.; Poduslo, S. E. Myelination in Rat Brain: Changes in Myelin Composition During Brain Maturation. *J. Neurochem.* **1973**, *21* (4), 759–773. https://doi.org/10.1111/j.1471-4159.1973.tb07520.x.

(47) Hoshi, M.; Williams, M.; Kishimoto, Y. Characterization of Brain Cerebrosides at Early Stages of Development in the Rat. *J. Neurochem.* **1973**, *21* (3), 709–712. https://doi.org/10.1111/j.1471-4159.1973.tb06017.x.

(48) Eckhardt, M.; Yaghootfam, A.; Fewou, S. N.; Zöller, I.; Gieselmann, V. A Mammalian Fatty Acid Hydroxylase Responsible for the Formation of α-Hydroxylated Galactosylceramide in Myelin. *Biochem. J.* **2005**, *388* (1), 245–254. https://doi.org/10.1042/BJ20041451.

(49) Ivanova, P. T.; Cerda, B. A.; Horn, D. M.; Cohen, J. S.; McLafferty, F. W.; Brown, H. A. Electrospray Ionization Mass Spectrometry Analysis of Changes in Phospholipids in RBL-2H3 Mastocytoma Cells during Degranulation. *Proc. Natl. Acad. Sci. U. S. A.* **2001**, *98* (13), 7152–7157. https://doi.org/10.1073/pnas.131195098.

(50) Cajka, T.; Fiehn, O. Toward Merging Untargeted and Targeted Methods in Mass Spectrometry-Based Metabolomics and Lipidomics. *Anal. Chem.* **2016**, *88* (1), 524–545. https://doi.org/10.1021/acs.analchem.5b04491.

(51) Pintado-Sierra, M.; García-Álvarez, I.; Bribián, A.; Medina-Rodríguez, E. M.; Lebrón-Aguilar, R.; Garrido, L.; de Castro, F.; Fernández-Mayoralas, A.; Quintanilla-López, J. E. A Comprehensive Profiling of Sulfatides in Myelin from Mouse Brain Using Liquid Chromatography Coupled to High-Resolution Accurate Tandem Mass Spectrometry. *Anal. Chim. Acta* **2017**, *951*, 89–98. https://doi.org/10.1016/j.aca.2016.11.054.

(52) Gaudin, M.; Imbert, L.; Libong, D.; Chaminade, P.; Brunelle, A.; Touboul, D.; Laprévote, O. Atmospheric Pressure Photoionization as a Powerful Tool for Large-Scale Lipidomic Studies. *J. Am. Soc. Mass Spectrom.* **2012**, *23* (5), 869–879. https://doi.org/10.1007/s13361-012-0341-y.

(53) Mikula, S.; Trotts, I.; Stone, J. M.; Jones, E. G. Internet-Enabled High-Resolution Brain Mapping and Virtual Microscopy. *Neuroimage* **2007**, *35* (1), 9–15. https://doi.org/10.1016/j.neuroimage.2006.11.053.

(54) Shariatgorji, M.; Nilsson, A.; Goodwin, R. J. A.; Källback, P.; Schintu, N.; Zhang, X.; Crossman, A. R.; Bezard, E.; Svenningsson, P.; Andren, P. E. Direct Targeted Quantitative Molecular Imaging of Neurotransmitters in Brain Tissue Sections. *Neuron* **2014**, *84* (4), 697–707. https://doi.org/10.1016/j.neuron.2014.10.011.

(55) Decavel, C.; Van Den Pol, A. N. GABA: A Dominant Neurotransmitter in the Hypothalamus. *J. Comp. Neurol.* **1990**, *302* (4), 1019–1037. https://doi.org/10.1002/cne.903020423.

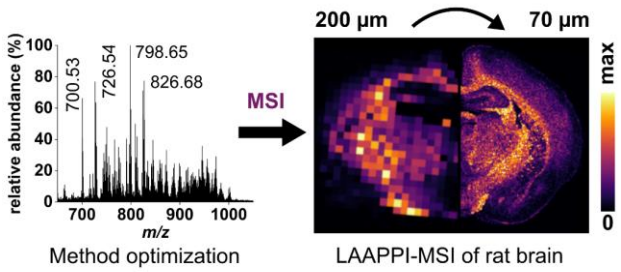

Method optimization LAAPPI-MSI of rat brain

Supporting Information for

Sub-100 µm spatial resolution ambient mass spectrometry imaging of rodent brain with laser ablation atmospheric pressure photoionization (LAAPPI) and laser ablation electrospray ionization (LAESI)

Juha-Pekka Hieta[†], Jaakko Kopra[‡], Heikki Räikkönen[†], Tiina J. Kauppila[§*], Risto Kostiainen[†*]

[†]Drug Research Program and Division of Pharmaceutical Chemistry and Technology, Faculty of Pharmacy, P.O. Box 56, FI-00014 University of Helsinki, Finland

[‡]Division of Pharmacology and Pharmacotherapy, Faculty of Pharmacy, P.O. Box 56, FI-00014 University of Helsinki, Finland

[§]Finnish Institute for the Verification of the Chemical Weapons Convention (VERIFIN), Department of Chemistry, P.O. Box 55, FI-00014 University of Helsinki, Finland

Correspondence: risto.kostiainen@helsinki.fi, tiina.kauppila@helsinki.fi

Table of Contents

Imaging setup

The mass spectrometer was equipped with in-house-built LAAPPI and LAESI sources as described below. The sample glass slides were mounted on a sample holder that was attached to a computer controllable X-Y-Z translation stage (NRT100/M; Thorlabs, Newton, MA, USA). The sample holder consisted of two Peltier elements (TES1-12703; Hebei, Shanghai, China) in parallel configuration, in-house-built, and water-cooled aluminum heatsink, and PT100 (ETP-RT-4-24-PT100B, Variohm) and NTC (B57045-K103-K; EPCOS) temperature sensors that were attached to the holder surface and the heatsink, respectively. The Peltier elements were precision-driven with a thermoelectric cooler (TEC) controller (TEC-1090-HV; Meerstetter Engineering, Switzerland). The temperature of the holder surface was always kept below -20 °C to decrease the rate of dehydration and enzymatic and chemical reactions such as oxidation in tissue.

The tissue sections were photographed from above with a Dino-Lite microscope camera (AM7915MZT, AnMo Electronics, New Taipei City, Taiwan) before and after analysis. The camera also captured a live video feed of the sample region, which permitted the selection of polygon-shaped areas for MSI measurements. The live feed was combined with a coordinate system that was synchronized with the sample holder coordinates (x, y) based on the focal point of the laser beam. The coordinate system was created using the known coordinates of at least three laser-ablated holes in tissue or any other medium as basis. The tissue sections were always fixed (roughly) to the same region of the microscope glass slide, which enabled the use of the same coordinate system from sample to sample as the camera was kept at the same position with respect to the sample holder. Regardless, the sample area was also selected with a small extra margin to ensure that the entire region of interest was always analyzed in case of a small offset in the coordinate system.

The entire imaging setup was built on an aluminum optical breadboard plate (MB6090/M; Thorlabs) mounted on a rigid support frame (PFM52501; Thorlabs) and was enclosed with clear acrylic boards using aluminum rails as a supporting structure (as XE25C10D; Thorlabs). The mass spectrometer side of the enclosure was left open and extra acrylic extension boards were attached to this opening to enable the mounting of the entire setup to any mass spectrometer as a removable module. The setup was semi-closed to control the relative humidity of the sample region with dry nitrogen flow and to prevent contamination of the laboratory by the biological samples. The nitrogen environment prevented excess condensation of water on the cooled samples and decreased the risk of discharge in negative electrospray ionization (ESI). The relative humidity inside the module was measured using a Vaisala HMP231 transmitter.

A part of the casing was also required to transmit IR light (2.94 µm) emitted by an OPOTEK IR Opolette HE 2940 (Carlsbad, CA, USA) laser that had a maximum repetition rate and output energy of 20 Hz and 6 mJ, respectively. Thus, a section of the acrylic board on top of the sampling area was replaced with a CaF_2 window (WG51050-D; Thorlabs) that allowed >90% transmittance of the emitted 2.94-µm IR laser wavelength. A rigid mirror holder setup was attached to the window holder frame (VPCH512; Thorlabs) on top of the window to reflect the emitted laser beam (approximately) perpendicular to the sample. The IR laser beam was guided to this mirror through a simple mirror setup described previously.[1] The mirror setup permitted setting of a specific sampling spot diameter (20–200 µm) by solely changing the beam travel distance prior to the focusing lens (PF10-03-M01; Thorlabs). Here, spot diameter of approximately 65 µm was selected due to its suitable accuracy for showing the structural details of rodent brain in a reasonable measurement timeframe.

LAAPPI and LAESI ion sources

With both ion sources, the mass spectrometer inlet glass capillary was equipped with a 24-mm long stainless-steel (SS) extension capillary with an internal diameter (I.D.) of 0.79 mm (1/32”). A resistance wire (4.68 Ω/m) with an insulating fiberglass sleeving (FBGS; OMEGA Engineering, Norwalk, CT, USA) was twisted tightly around the SS capillary to cover its whole length. The surface of the tip, however, was left uncovered to ensure the functionality of the capillary as a counter electrode for electrospray. The resistance wire was attached to a computer-controlled power supply (ISO-TECH IPS-603; Aim & Thurlby Thandar Instruments, Huntington, United Kingdom) to set a suitable capillary temperature for assisting the desolvation of ions. Thus, the conventionally used heated nitrogen counterflow was not required or used. Capillary temperatures of 370 °C and 200 °C were used for LAAPPI and LAESI-MS, respectively.

The LAAPPI source consisted of a krypton discharge vacuum ultraviolet (VUV) photoionization lamp (PKR 100; Heraeus Noblelight, Cambridge, UK) and a SS pneumatic sprayer. The sprayer consisted of a Swagelok tee, two SS capillaries of I.D./O.D. 101.6/228.6 and 254/1587.5 µm, a nitrogen gas line, and ferrules for connections. The inner SS capillary protruded 0.3–0.5 mm from the outer one. The outer SS capillary was heated using a resistance wire, similarly as described above for the extension capillary. The spray solvent (acetone, toluene or chlorobenzene) was pumped through the inner SS capillary and nebulizer gas (nitrogen) was introduced between the inner and outer SS capillaries. The heated sprayer produced a hot vapor jet that was directed towards the ablation plume and the heated extension capillary at the mass spectrometer inlet. The jet was produced using several spray solvent flow rates, nitrogen gas pressures, and temperatures; 1–5 µL min^{-1}, 0.4–0.8 MPa, and 300–450 °C, respectively, were found to be optimal for brain tissue analysis. The VUV lamp emitted 10.0- and 10.6-eV photons and was positioned orthogonally to the extension capillary using the closest feasible distance to the plume and spray without blocking the IR laser beam.

The LAESI source consisted of a 100-µm I.D. SS electrospray needle (MT320-100-5-5; New Objective, MA, US) and a 101.6-µm SS capillary attached to the opposite end of the PEEK union with a suitable FEP sleeve. The latter capillary was connected to a solvent line and to a home-built high voltage power supply. The applied voltage of (+/–) 2.1–2.3 kV was selected to produce a steady cone-jet mode of electrospray. The spray was directed towards the ablation plume and the extension capillary under the nitrogen environment.

Optimization of LAAPPI- and LAESI-MS for brain tissue analysis

The effects of ablation and ionization parameters were investigated to achieve maximum sensitivity and stability in MSI of the mouse brain using LAAPPI- and LAESI-MS. These parameters were 1) positioning of the sprayer tip, the sampling spot, and the extension capillary in relation to each other; 2) the spray solvent and its flow rate and the pressure and temperature of the nebulizer gas (nitrogen); and 3) the thickness and temperature of the sample and its state prior to analysis. All optimized ion source settings are summarized in Table 1.

Sampling geometry

With LAAPPI and LAESI sources, where the IR laser beam was focused to the surface of the sample as perpendicular as possible, the optimal distance between the extension capillary inlet and the sampling spot (distance x_1 in Figure 1) was approximately 4–6 mm. When the distance x_1 was decreased below 4 mm, the ion transfer efficiency into MS began to decrease as a part of the IR ablation plume ended up behind the extension capillary inlet. The signal intensities also decreased with excess distance ($x_1 > 6$ mm) due to the decreased sampling efficiency of the spray. The results indicate that the sampling spot should be positioned such that the edge of the IR ablated plume is as close as possible to the extension capillary inlet and such positioning likely applies regardless of the sampling geometry.

The optimal distance between the extension capillary inlet axis and the sample surface (distance z_1 in Figure 1) for repeatable sampling was approximately 6–8 mm with both techniques. At larger distances ($z_1 > 8$ mm), an increased part of the compounds in the expanding ablated plume drifted outside of the ionization zone (solvent spray zone) resulting in a further decrease in sensitivity and repeatability. Smaller distances ($z_1 < 6$ mm) increased the risk of undesired melting of the frozen sample due to the heat emitted by the extension capillary or the APPI sprayer. Thermal or spray desorption was not observed at the optimal z_1 distances.

In LAAPPI- and LAESI-MS, the best sensitivity was achieved when the position of the sprayer was on-axis in relation to the extension capillary and at a distance of 1 mm from the sampling spot (distance x_2 in Figure 1). However, at a distance of 1 mm, the LAESI emitter operated either in pure ESI mode or ion spray mode (pneumatically assisted ESI) was prone to adsorption of ablated brain tissue residues that slowly accumulated on the ESI emitter tip over time. Such accumulation causes carry-over that results in prolonged signal durations and total MSI measurement times. A dwell time of 4–6 s was required to avoid all memory effects from one spot with a flow rate of 3.0 µL min^{-1} (Figure S2). Contamination of the ES emitter tip may also ultimately destabilize the electrospray or change the direction of the electrospray in long-lasting MSI measurements, which both result in decreased spot-to-spot repeatability. To avoid these problems, the tip of the ESI emitter should be positioned at a distance greater than 1 mm from the sampling spot. However, this results in reduced sensitivity. These problems were not observed with LAAPPI, since APPI uses a heated nebulizer. Therefore, the APPI sprayer can be positioned at an optimal x_2 distance (1 mm) to achieve maximum sensitivity. In LAAPPI, where carry-over is negligible, signal durations varied between 0.6–1.2 s (3–6 scans) with a data acquisition frequency of 5 Hz. However, the rate of pixel acquisition is currently limited by the developed MATLAB-based imaging software as, e.g., the laser triggering process alone takes about 0.8 s. Thus, a dwell time of ~3.0 s was used with LAAPPI-MSI as it is currently the shortest feasible.

Spray formation

The spray solvent in LAAPPI and LAESI had a significant effect on the detected ions and their intensities. In LAAPPI, the ionization mechanism is dependent on the spray solvent used. Similarly, as previously reported with APPI,[2,3] toluene and chlorobenzene (PhCl) are able to ionize compounds via

proton transfer or via charge exchange reactions, whereas only proton transfer reactions are possible with acetone. This was demonstrated in the detection of cholesterol in brain samples (Figure S1). Using chlorobenzene, cholesterol produced molecular ion at *m/z* 386 via a charge exchange reaction, protonated molecule via proton transfer reaction at *m/z* 387, and fragments $[M–H_2O]^{+\cdot}$ at *m/z* 368 and $[M+H–H_2O]^+$ at *m/z* 369. The mass peak at *m/z* 387 cannot be separated from the first isotope peak at *m/z* 386, but the intensity of m/z 387, is about 38.7% of the intensity of *m/z* 386, which is larger than the theoretical 29.9% calculated for the first isotope mass peak, suggesting that cholesterol is also partly ionized by proton transfer reaction producing a relatively weak protonated molecule by LAAPPI-MS. Using acetone, the spectrum showed a weak protonated molecule and abundant fragment $[M+H–H_2O]^+$ at *m/z* 369 and no molecular ion was formed. LAESI produced only the fragment ion $[M+H–H_2O]^+$ at *m/z* 369.There was also a significant difference between the sensitivities of LAAPPI- and LAESI-MS, as LAAPPI-MS shows almost one order of magnitude higher intensity for the main cholesterol peak (*m/z* 369). These results show that non-polar neutral compounds, which may be poorly ionized by ESI or where a molecular weight diagnostic ion is not formed, can be efficiently ionized via a charge exchange reaction by APPI using PhCl as a spray solvent. In LAESI, the compounds in the ablated plume must be first dissolved to charged droplets after which they are ionized similarly as in conventional ESI. To ensure dissolution of a large range of compounds, including lipids, an 8:1 MeOH:H_2O mixture was selected for LAESI-MS. A relatively high concentration of MeOH produced stable electrospray in positive and in negative ion modes and enhanced ionization efficiency (and thus sensitivity) as reported earlier.[4]

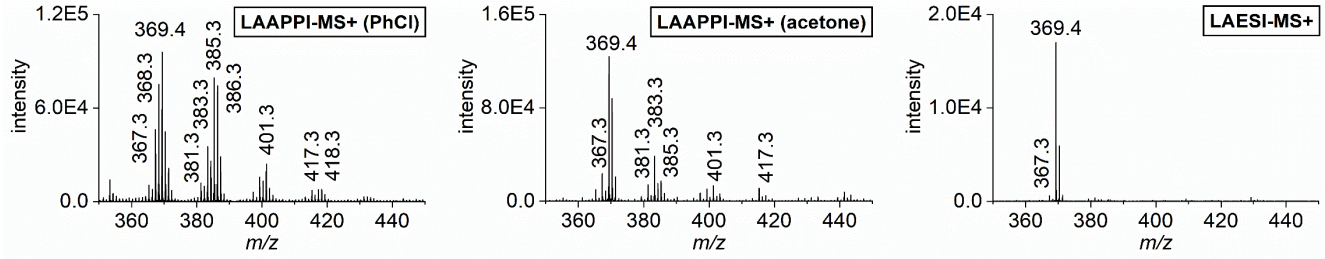

Figure S1. The effect of ionization technique on the detection of cholesterol measured by LAAPPI- and LAESI-MS with equal MS settings.

The spray solvent flow rates in LAESI and LAAPI were tested with flow rates of 1–3 µL min^{-1} and 1–5 µL min^{-1}, respectively. Increasing the flow rate from 1.0 to 3.0 µL min^{-1} in LAESI decreased the signal durations from over 10 s to 4–6 s when the ES emitter was placed close to the ablation plume to obtain the best sensitivity (Figure S2). An increased flow rate enhanced flushing of the emitter tip and formed a wider spray to protect the emitter tip from contaminants that could cause a decrease in signal durations. The signal heights and thus sensitivity also increased 2–3 fold when the flow rate was increased from 1.0 to 3.0 µL min^{-1} (Figure S2). The flow rate, however, also affects the stability of pure electrospray and good stability of ESI was achieved with flow rates up to 3.0 µL min^{-1}. Thus, the solvent flow rate of 3.0 µL min^{-1} was selected for LAESI-MSI measurements. In LAAPPI-MS, the increase in flow rate from 1 to 5 µL min^{-1} had no significant effect on sensitivity with acetone or PhCl. However, higher flow rates resulted in somewhat better spot-to-spot repeatability as shown with the smaller standard deviations of cholesterol signals (Figure S3). However, an increase in APPI spray solvent flow rate also resulted in higher background.

As LAAPPI-MS utilizes a heated spray, the effect of temperature of the solvent spray on acquired signal intensities was tested in the region of 250–550 °C (Figure S4). The temperature of the solvent spray was measured at close proximity to the sprayer nozzle, and it was recognized that temperatures between 250–450 °C had no significant effect on signal intensities. However, signals were decreased at 500 °C, possible due to thermal degradation of the compounds. To achieve efficient vaporization of the spray

solvent and to avoid possible thermal degradations, a temperature of 350 °C was found to be optimal in LAAPPI-MSI.

Sample thickness and temperature

The effect of sample thickness on acquired signals was tested with 20-, 40-, and 60-µm thick mouse brain tissue sections. When the section thickness increased from 20 to 60 µm, the average total intensities acquired by LAAPPI-MS increased about two-fold whereas no such increase in signal intensity was observed with LAESI-MS (Figure S5). The observed differences in sensitivities between LAESI and LAAPPI with 20-µm and 40-µm tissue sections may be due to the differences in dissolution of the ablated tissue projectiles to the spray solvent used. As LAESI-MS with 20-µm sections provided a similar sensitivity as thicker sections and contamination of an ES emitter or the MS inlet was less with 20-µm than with 40-µm sections, 20-µm sections were used in LAESI-MSI. In LAAPPI-MSI experiments, there was no contamination of the sprayer even with 40-µm thick sections, which could result from the high vapor temperature of 300–500 °C when compared to ES operated at ambient temperature. In LAAPPI-MSI, maximum sensitivity can be obtained with 40-µm sections, but 20-µm sections could be used to minimize possible contamination of the MS site.

The IR ablation process is dependent on the sample temperature adjusted by the temperature of the Peltier elements at the sample holder. Low temperatures (–20 to –25 °C) were preferred as the diffusion rate of metabolites and their enzymatic or chemical reactions in the tissue are decreased at lower temperatures. It was also observed that sampling of frozen tissue resulted in a plume consisting of finer tissue particles compared to those formed from an unfrozen sample. Ablation of finer particles particularly improved sampling repeatability in LAESI-MS experiments as larger tissue particles decreased the stability of the spray. Spot-to-spot repeatability was also dependent on the amount of water on the sample surface. Therefore, the rate of sublimation and condensation (i.e. formation of ice crystals) of water should be in equilibrium to prevent dehydration of sample or accumulation of ice on the sample surface during long-lasting MSI experiments. Thus, the sample temperature should be adjusted according to the relative humidity within the setup module and the temperatures of the extension capillary and the APPI nebulizer in LAAPPI. In LAESI-MSI, when the sample holder and extension capillary temperatures were set to –22 °C and 200 °C, respectively, a relative humidity of 3–4 % was adjusted with nitrogen in the module, whereas a larger relative humidity of 6–7 % was set in LAAPPI-MSI when the capillary extension and APPI nebulizer temperatures were 350 °C.

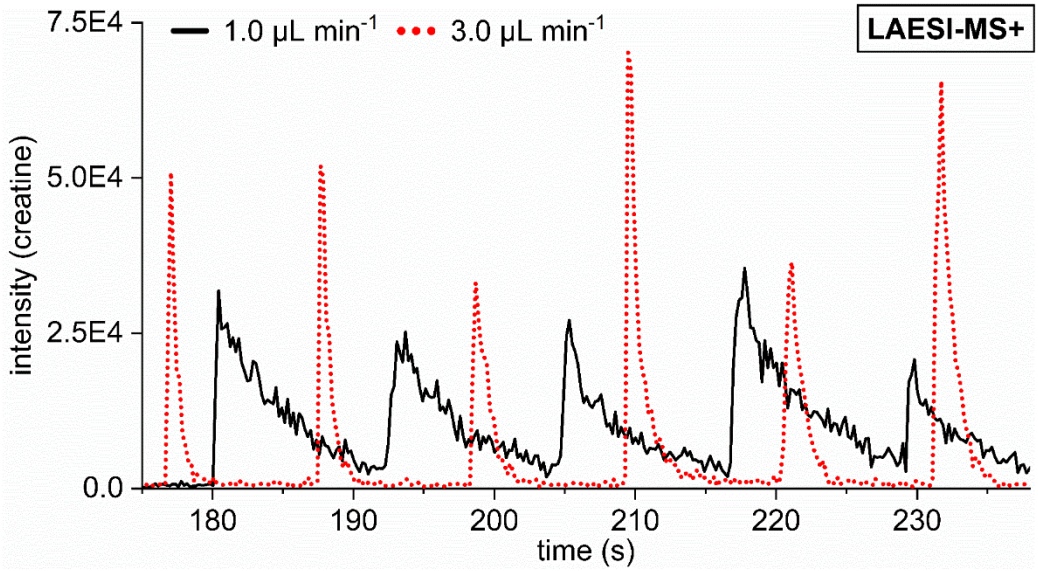

Figure S2. The effect of ESI solvent flow rate (1.0 and 3.0 µL min^{-1}) on carry-over in the LAESI-measurement of creatine detected as $[M+H]^+$ at *m/z* 132.08 in mouse brain by positive ion LAESI-MS.

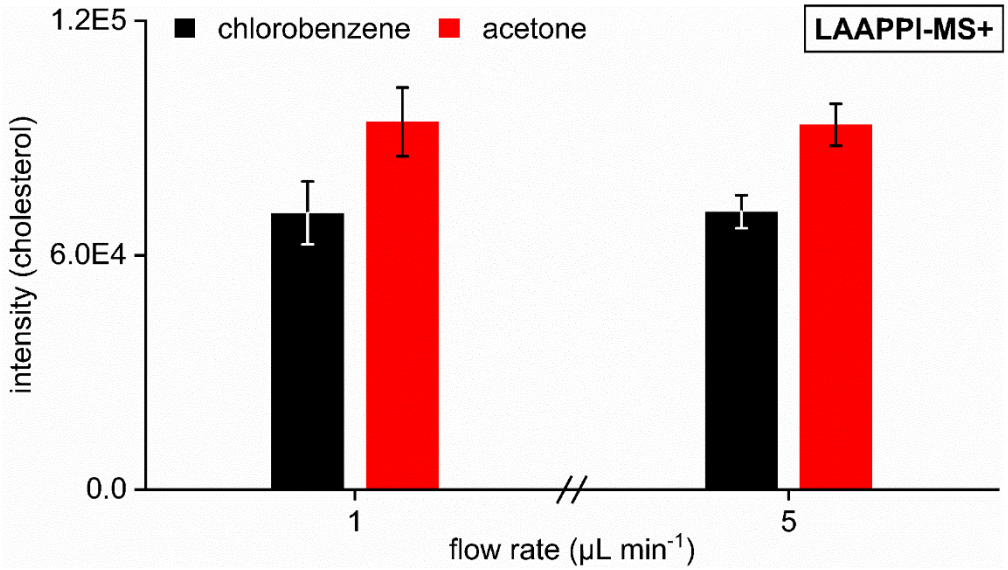

Figure S3. The effect of spray solvent (chlorobenzene or acetone) flow rate on the intensity (the mean of eight measurements ± standard deviation) of cholesterol detected as $[M+H–H_2O]^+$ at *m/z* 369.35 in positive ion LAAPPI-MS.

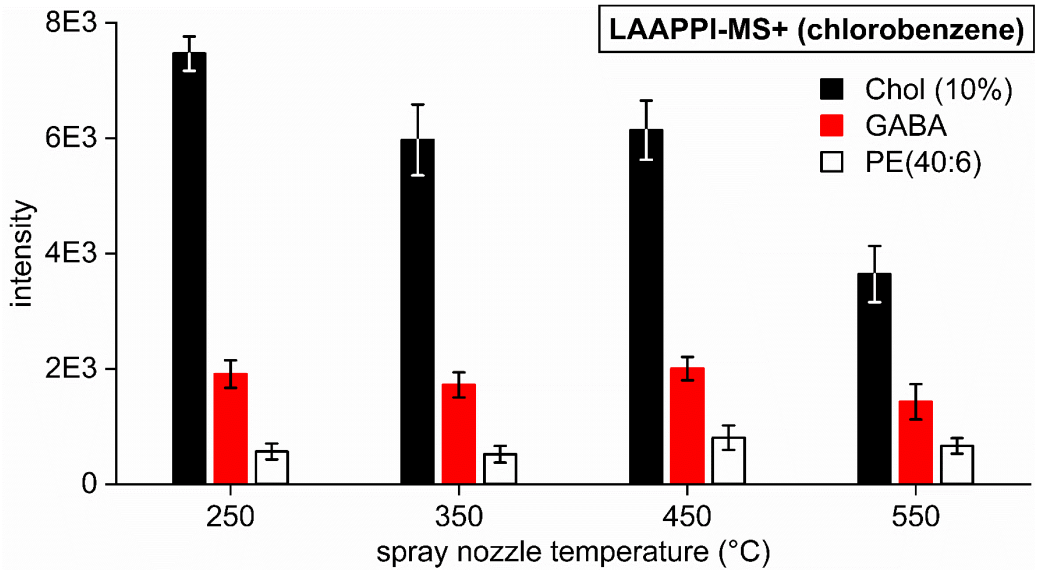

Figure S4. The effect of spray nozzle temperature on the intensities of (the mean of eight measurements ± standard deviation) of cholesterol ($[M–H_2O]^{+\cdot}$ at *m/z* 368.34), γ-aminobutyric acid (GABA) ($[M+H]^+$ at *m/z* 104.07), and phosphatidylethanolamine PE(40:6) ($[M+H]^+$ at *m/z* 792.55) measured by positive ion LAAPPI-MS with chlorobenzene as a spray solvent.

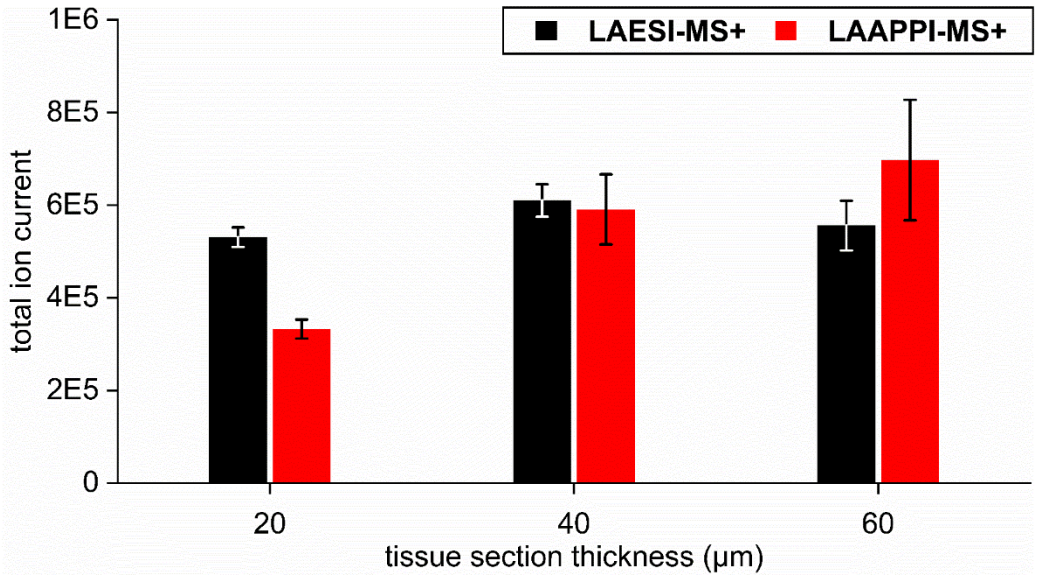

Figure S5. The effect of tissue section thickness on the intensities of TIC signals (the mean of eight measurements ± standard deviation) measured by positive ion LAAPPI- and LAESI-MS.

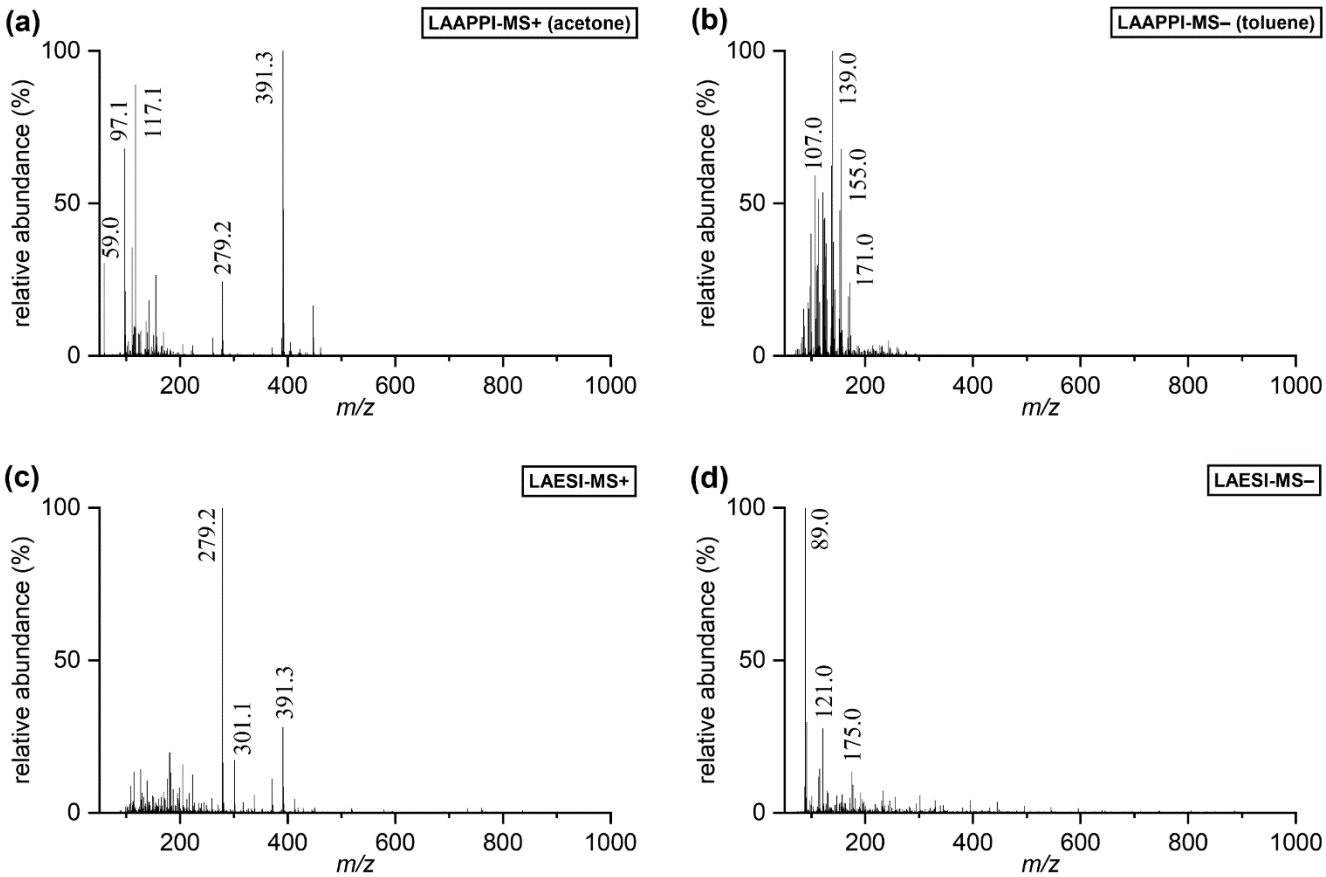

Figure S6. Typical background spectra acquired by positive and negative ion LAAPPI- and LAESI-MS. For example, major phthalate peaks at *m/z* 279.2 and 391.3 are present in both positive ion spectra and acetone and its dimer peak are present at *m/z* 59.0 and 117.1 in the positive ion LAAPPI-MS spectrum. Negative ion LAAPPI-MS had the largest background at the mass range below *m/z* 200 due to contamination, whereas the background of negative ion LAESI-MS was the lowest of all four methods.

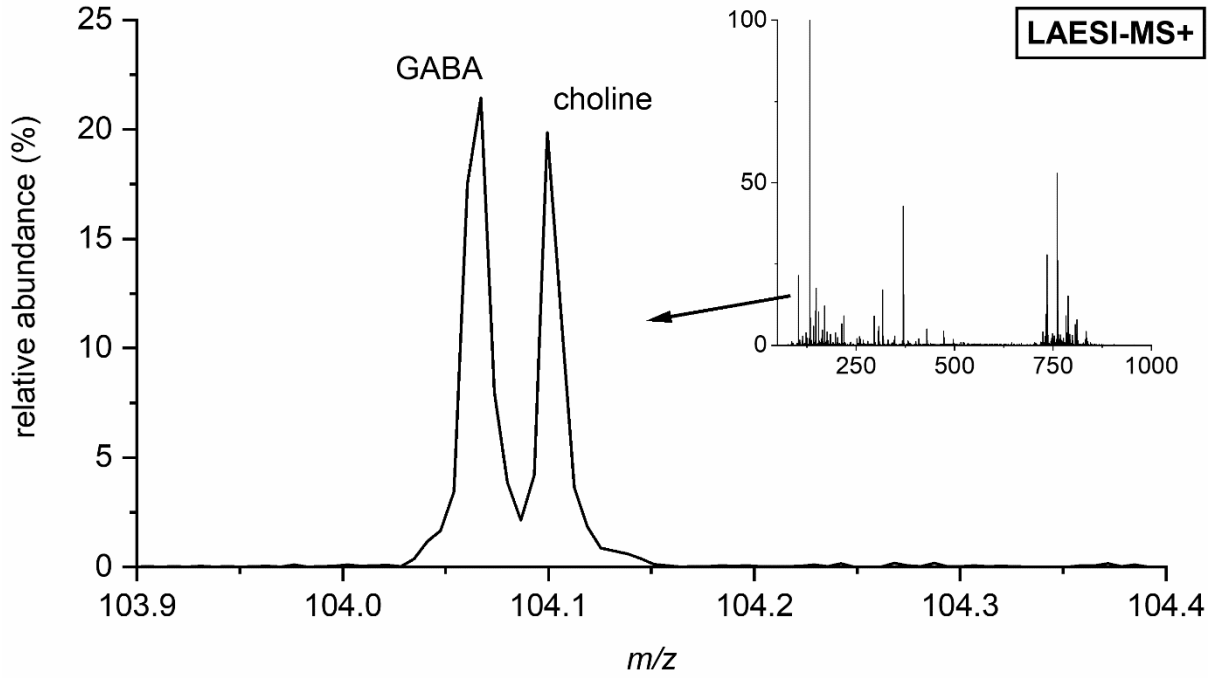

Figure S7. Positive ion LAESI-MS mass spectrum showing separated mass peaks of GABA and choline detected as $[M+H]^+$ and M^+ at *m/z* 104.07 and 104.10, respectively. The relative abundances of the two mass peaks varies depending on the analyzed brain region. The presented spectrum is similar to the one shown previously by Nemes et al.[5] In contrast to LAESI-MS, positive ion LAAPPI-MS shows only one mass peak at *m/z* 104.07.

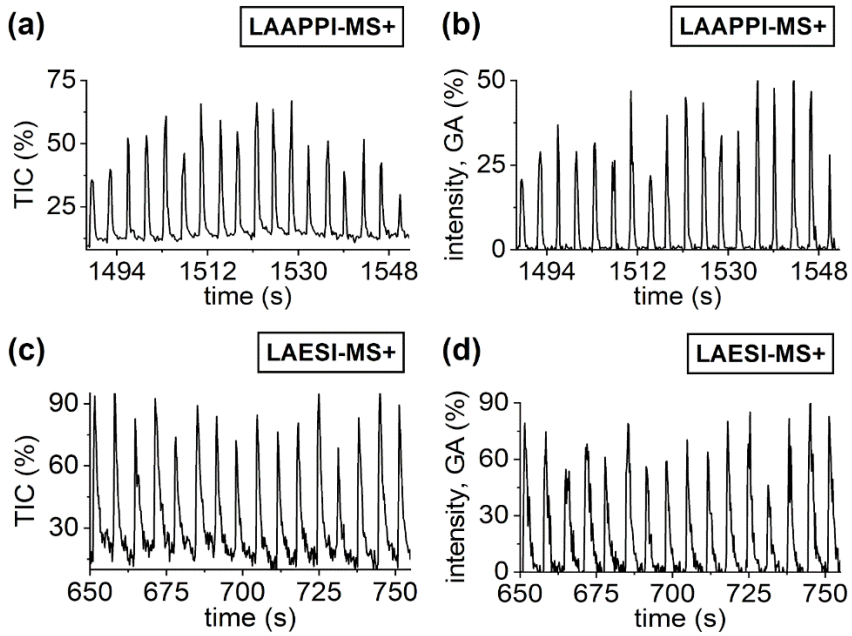

Figure S8. Partial total ion current (TIC) traces in (a) and (c) and selected ion traces of glutamic acid (GA) in (b) and (d) acquired from mouse brain tissue by positive ion LAAPPI- and LAESI-MS. The average TIC peak intensities of LAAPPI- (n = 18) and LAESI-MS (n = 16) were approximately 1.6E6 and 4.3E5 with relative standard deviations of 16.8% and 4.2%, respectively.

Table S1. Proposed identities of brain metabolites and lipids for the main ions detected with mass error < 30 ppm by positive and negative ion LAAPPI- and LAESI-MS, mass errors and relative abundances rated with symbols of a star (* < 5%, ** = 5–30%, *** > 30 %). The mass resolution of the instrument was approximately 10000.

Proposed compound	MW	Detected ions mass errors (ppm) (LAAPPI / LAESI)		Abundance Positive ions		Abundance Negative ions	
		positive	negative	LAAPPI	LAESI	LAAPPI	LAESI
Alanine	89.048	–	$[M–H]^-$	–	–	**	**
		–	-22.7 / 6.8				
Lactic acid	90.032	–	$[M–H]^-$	–	–	***	***
		–	-22.5 / 6.9				
Phosphate	97.977	–	$[M–H]^-$	–	–	–	***
		–	– / 14.4				
GABA	103.063	$[M+H]^+$	$[M–H]^-$	*	**	**	**
		3.8 / 13.5	-19.6 / 8.8				
Choline	104.108	M^+	–	–	**	–	–
		– / -14.4	–				
Serine	105.043	–	$[M–H]^-$	*	*	**	*
		–	-19.2 / 6.7				
Threonine / Homoserine	119.058	–	$[M–H]^-$	*	*	*	*
		–	-25.4 / 8.5				
Taurine	125.015	$[M+H]^+$	$[M–H]^-$	–	*	–	***
		– / -7.1	– / 29				
Creatine	131.069	$[M+H]^+$	$[M–H]^-$	**	***	**	**
		-6.1 / -6.1	-23.1 / -9.2				
Aspartic acid	133.038	$[M+H]^+$	$[M–H]^-$	*	**	**	**
		16.4 / -13.4	-7.6 / -16.7				
Adenine	135.055	$[M+H]^+$	$[M–H]^-$	*	–	**	–
		-5.9 / –	-14.9 / –				
Spermidine	145.158	$[M+H]^+$	–	*	*	–	–
		-15.1 / 19.2	–				
Glutamine	146.069	$[M+H]^+$	$[M–H]^-$	**	**	**	**
		4.1 / -16.3	-6.9 / 21.4				
Glutamic acid	147.053	$[M+H]^+$	$[M–H]^-$	**	***	***	***
		4.1 / -16.2	20.5 / 28.1				
N-Acetyl-L-aspartic acid	175.048	$[M+H]^+$	$[M–H]^-$	*	*	**	***
		4.0 / -18.7	-16.1 / -16.7				
Ascorbic acid	176.032	–	$[M–H]^-$	–	–	–	***
		–	– / -4.6				
Hexose	180.063	–	$[M–H]^-$	–	–	**	*
		–	-11.2 / 16.2				
Spermine	203.224	$[M+H]^+$	–	**	**	–	–
		-9.8 / 9.8	–				
L-Aspartyl-4-phosphate	213.004	$[M+H]^+$	–	–	**	–	–
		– / -9.3	–				

Proposed compound	MW	Detected ions mass errors (ppm) (LAAPPI / LAESI)		Abundance Positive ions		Abundance Negative ions	
		positive	negative	LAAPPI	LAESI	LAAPPI	LAESI
Adenosine	268.105	$[M+H]^+$	–	**	**	–	–
		11.2 / 7.5	–				
Glutathione	307.084	$[M+H]^+$	$[M–H]^-$	–	**	–	**
		– / -6.5	– / 3.3				
Adenosine monophosphate	347.071	$[M+H]^+$	$[M–H]^-$	–	*	–	**
		– / -5.7	– / -16.1				
Cholesterol	369.352	$[M+H–H_2O]^+$	–	***	***	–	–
		-3.2 / -3.2	–				
PE(P-34:1)	701.536	$[M+H]^+$	$[M–H]^-$	**	*	***	**
		8.3 / -11.7	-2.4 / -12.4				
SM(d34:1)	702.568	$[M+H]^+$	–	–	*	–	–
		– / 5.8	–				
PE(34:0)	719.547	$[M+H]^+$	$[M–H]^-$	**	*	**	**
		4.4 / -12.2	1.1 / -11.4				
PE(P-36:4)	723.520	$[M+H]^+$	$[M–H]^-$	**	*	***	***
		-11.9 / -6.3	2.8 / 2.8				
PE(P-36:2)	727.552	$[M+H]^+$	$[M–H]^-$	***	*	***	***
		-2.6 / -16.3	2.3 / -1.8				
SM(d36:2)	728.583	$[M+H]^+$	–	–	*	–	–
		– / -15.8	–				
PE(P-36:1)	729.567	$[M+H]^+$	$[M–H]^-$	***	*	***	**
		6.2 / -4.8	-9.6 / -8.2				
SM(d36:1)	730.599	$[M+H]^+$	–	–	**	–	–
		– / -5.7	–				
PC(32:0)	733.562	$[M+H]^+$	–	–	***	–	–
		– / 0.8	–				
PE(36:4)	739.515	$[M+H]^+$	$[M–H]^-$	*	*	**	**
		-3.4 / 7.4	2.8 / 1.5				
PE(36:2)	743.547	$[M+H]^+$	$[M–H]^-$	*	*	**	**
		1.6 / 9.7	-1.6 / 9.2				
PE(36:1) / PE-NMe2(34:1)	745.562	$[M+H]^+$	$[M–H]^-$	**	*	***	***
		-11.3 / 26.3	-20.0 / -16.0				
PE(P-38:6)	747.520	$[M+H]^+$	$[M–H]^-$	*	*	***	***
		-20.8 / -14.2	9.4 / -5.4				
PE(P-38:5)	749.536	$[M+H]^+$	$[M–H]^-$	**	*	***	***
		-4.3 / 9.1	1.7 / -0.9				
PE(P-38:4)	751.552	$[M+H]^+$	$[M–H]^-$	**	*	***	***
		16.1 / -5.2	2.3 / -13.7				
PE(P-38:2)	755.583	$[M+H]^+$	$[M–H]^-$	**	*	***	**
		2.4 / -6.9	1.9 / -7.4				

Proposed compound	MW	Detected ions mass errors (ppm) (LAAPPI / LAESI)		Abundance Positive ions		Abundance Negative ions	
		positive	negative	LAAPPI	LAESI	LAAPPI	LAESI
SM(d38:1)	758.630	$[M+H]^+$	–	–	*	–	–
		– / -12.5	–				
PC(34:1)	759.578	$[M+H]^+$	–	–	***	–	–
		– / 1.2	–				
PE(38:6)	763.515	$[M+H]^+$	$[M-H]^-$	**	–	***	**
		3.3 / –	10.6 / -10.4				
PE(38:4) / PE-NMe2(36:4)	767.547	$[M+H]^+$	$[M-H]^-$	**	*	***	***
		0.3 / -8.8	6.3 / -9.4				
PE(P-40:6)	775.552	$[M+H]^+$	$[M-H]^-$	**	*	***	***
		6.6 / 2.7	7.4 / -4.3				
PE(P-40:5)	777.567	$[M+H]^+$	$[M-H]^-$	**	*	***	**
		10.9 / -14.8	-12.9 / -18.0				
PC(36:4)	781.562	$[M+H]^+$	–	–	**	–	–
		– / -18.4	–				
GalCer(d40:2) / GalCer(d40:1(OH)) (pos)	781.643	$[M+H]^+$ / $[M+H-H_2O]^+$	$[M-H]^-$	***	–	**	–
		-6.9 / –	0.8 / –				
GalCer(d40:2)	781.643	–	$[M+Cl]^-$	–	–	**	**
		–	8.5 / -6.1				
GalCer(d40:1)	783.659	$[M+H]^+$	$[M-H]^-$	**	–	**	–
		-2.7 / –	-4.5 / –				
GalCer(d40:1)	783.659	–	$[M+Cl]^-$	–	–	**	**
		–	-6.9 / 1.6				
PC(36:1)	787.609	$[M+H]^+$	–	–	**	–	–
		– / -10.7	–				
PS(36:1)	789.552	–	$[M-H]^-$	–	–	–	***
		–	– / -11.0				
PE(40:6) / PE-NMe2(38:6) / PC(37:6)	791.547	$[M+H]^+$	$[M-H]^-$	**	*	***	***
		2.8 / 4.0	8.6 / 18.7				
PE(40:4)	795.578	$[M+H]^+$	$[M-H]^-$	**	*	**	***
		-1.4 / -5.1	-13.2 / -17.0				
GalCer(d40:2(OH))	797.638	$[M+H]^+$	$[M-H]^-$	**	–	***	–
		7.0 / –	-3.5 / –				
GalCer(d40:1(OH))	799.654	$[M+H]^+$	$[M-H]^-$	***	–	***	–
		-3.7 / –	8.1 / –				
PC(38:6)	805.562	$[M+H]^+$	–	–	**	–	–
		– / 5.7	–				
PC(38:4)	809.594	$[M+H]^+$	–	–	**	–	–
		– / -14.4	–				
GalCer(d42:2) / GalCer(d42:1(OH)) (pos)	809.674	$[M+H]^+$ / $[M+H-H_2O]^+$	$[M-H]^-$	***	–	***	–
		-2.8 / –	4.7 / –				

Proposed compound	MW	Detected ions mass errors (ppm) (LAAPPI / LAESI)		Abundance Positive ions		Abundance Negative ions	
		positive	negative	LAAPPI	LAESI	LAAPPI	LAESI
GalCer(d42:2)	809.674	–	$[M+Cl]^-$	–	–	***	***
		–	10.3 / 12.6				
PS(38:4)	811.536	–	$[M–H]^-$	–	–	–	**
		–	– / -3.8				
GalCer(d42:1)*	811.690	$[M+H]^+$	$[M–H]^-$	***	–	**	–
		2.5 / –	-3.5 / –				
GalCer(d42:1)	811.690	–	$[M+Cl]^-$	–	–	**	**
		–	-7.1 / -3.5				
PE(P-42:1) (/ GalCer(d4**1**:1))	813.661	$[M+H]^+$	$[M–H]^-$	***	–	***	–
		19.1 / –	13.7 / –				
PE(42:7)	817.562	–	$[M–H]^-$	–	–	–	**
		–	– / -19.5				
PE(42:5)	821.594	–	$[M–H]^-$	–	–	–	**
		–	– / -23.4				
PE(42:3)	823.609	–	$[M–H]^-$	–	–	–	**
		–	– / -10.7				
GalCer(d42:2(OH))	825.669	$[M+H]^+$	$[M–H]^-$	***	–	***	–
		-14.2 / –	9.6 / –				
GalCer(d42:2(OH))	825.669	–	$[M+Cl]^-$	–	–	–	***
		–	– / -7.0				
GalCer(d42:1(OH))	827.685	$[M+H]^+$	$[M–H]^-$	***	–	**	–
		0.8 / –	5.1 / –				
GalCer(d42:1(OH))	827.685	–	$[M+Cl]^-$	–	–	–	**
		–	– / -3.3				
PS(40:6)	835.536	–	$[M–H]^-$	–	–	–	***
		–	– / -0.1				
PE(P-44:4) (/ GalCer(d40:1(OH)))	835.645	–	$[M–H]^-$ (/ $[M+Cl]^-$)	–	–	**	***
		–	-10.4 / 1.6				
PA(46:1)	842.676	–	$[M–H]^-$	–	–	***	–
		–	-10.9 / –				
PE(44:2)	855.672	–	$[M–H]^-$	–	–	**	**
		–	6.6 / 3.0				
PI(36:4)	858.526	–	$[M–H]^-$	–	–	–	**
		–	– / 1.2				
PI(38:5)	884.541	–	$[M–H]^-$	–	–	–	**
		–	– / -7.5				
PI(38:4)	886.557	–	$[M–H]^-$	–	–	–	**
		–	– / 4.6				
ST(d42:2)	889.631	–	$[M–H]^-$	–	–	–	**
		–	– / -2.3				

References

(1) Hieta, J.-P.; Vaikkinen, A.; Auno, S.; Räikkönen, H.; Haapala, M.; Scotti, G.; Kopra, J.; Piepponen, P.; Kauppila, T. J. A Simple Method for Improving the Spatial Resolution in Infrared Laser Ablation Mass Spectrometry Imaging. *J. Am. Soc. Mass Spectrom.* **2017**, *28* (6), 1060–1065. https://doi.org/10.1007/s13361-016-1578-7.

(2) Kauppila, T. J.; Syage, J. A.; Benter, T. Recent Developments in Atmospheric Pressure Photoionization-Mass Spectrometry. *Mass Spectrom. Rev.* **2017**, *36* (3), 423–449. https://doi.org/10.1002/mas.21477.

(3) Kauppila, T. J.; Kersten, H.; Benter, T. The Ionization Mechanisms in Direct and Dopant-Assisted Atmospheric Pressure Photoionization and Atmospheric Pressure Laser Ionization. *J. Am. Soc. Mass Spectrom.* **2014**, *25* (11), 1870–1881. https://doi.org/10.1007/s13361-014-0988-7.

(4) Kostiainen, R.; Bruins, A. P. Effect of Solvent on Dynamic Range and Sensitivity in Pneumatically-Assisted Electrospray (Ion Spray) Mass Spectrometry. *Rapid Commun. Mass Spectrom.* **1996**, *10* (11), 1393–1399. https://doi.org/10.1002/(SICI)1097-0231(199608)10:11<1393::AID-RCM654>3.0.CO;2-V.

(5) Nemes, P.; Woods, A. S.; Vertes, A. Simultaneous Imaging of Small Metabolites and Lipids in Rat Brain Tissues at Atmospheric Pressure by Laser Ablation Electrospray Ionization Mass Spectrometry. *Anal. Chem.* **2010**, *82* (3), 982–988. https://doi.org/10.1021/ac902245p.